A FOSSIL DIATOM PERSPECTIVE FROM LAGO CIPRESES (51°S, SOUTHWESTERN PATAGONIA) ON THE HOLOCENE HISTORY OF THE SOUTHERN WESTERLY WINDS

Tesis

Entregada A La

Universidad De Chile

En Cumplimiento Parcial De Los Requisitos

Para Optar Al Grado De

Magíster en Ciencias Biológicas

Facultad De Ciencias

Por

Leonardo André Villacís Custodio

Noviembre, 2021

Director de Tesis

Dr. Patricio I. Moreno Moncada

FACULTAD DE CIENCIAS

UNIVERSIDAD DE CHILE

INFORME DE APROBACIÓN

TESIS DE MAGÍSTER

Se informa a la Escuela de Postgrado de la Facultad de Ciencias que la Tesis de Magíster presentada por el candidato

Leonardo André Villacís Custodio

Ha sido aprobada por la comisión de Evaluación de la tesis como requisito para optar al grado de Magíster en Ciencias Biológicas, en el examen de Defensa Privada de Tesis rendido el día

Director de Tesis:

Dr. Patricio Iván Moreno Moncada .....

Comisión de Evaluación de la Tesis

Dr. Rodrigo Patricio Villa-Martínez .....

Dr. Luis Felipe Hinojosa Opazo .....

DEDICATION

Dedico este escrito a lo que era mi Abuelo y que ahora circula quién sabe dónde.

BIOGRAPHY

The more I read about climate, the more confused I become. The more confused I become, the more interested I get.

I am daunted by the capacity of increasing societal complexity to impinge upon Earth system dynamics, but at the same time, comforted by the capacity of diatoms to live an oblivious and transient life, completely nonchalant about their essentiality to our aerobic/consumer subsistence.

ACKNOWLEDGEMENTS

Durante el transcurso de este magíster he sentido el apoyo constante de mi tutor Dr. Patricio Moreno que me ha abierto numerosas puertas académicas y me ha brindado conocimientos extensos en ámbitos científicos y prácticos (ej., cómo hacer nudos). Espero aplicar el rigor científico que tanto lo caracteriza en mi subsiguiente desarrollo profesional. También agradezco profundamente el tiempo que pude estar en el laboratorio de Dra. Nora Maidana, cuya ejemplar forma de ser y enseñar me ha hecho disfrutar mucho más el trabajar con diatomeas. Siempre estuvo dispuesta a aclarar cualquier inquietud o incertidumbre que surgiese. Esta tesis no hubiese sido posible sin la enfática ayuda de Carolina Díaz Pardo que repetidas veces, y bajo las menos que ideales condiciones pandémicas, me permitió usar las instalaciones de AMAKAIK para trabajar. También ha sido un apoyo significativo en el quehacer diatomístico. Similarmente, agradezco a Dámaris Méndez que siempre estuvo dispuesta a capacitar y a tutelar las jornadas en AMAKAIK. A todos y todas las presentes en el laboratorio de Dr. Patricio Moreno (Loreto Hernández, Javiera Videla, M. José Kaffman, Dra. Carla Henríquez, Dra. Lucía Guerra, Dalila Briones y Emilia Isadora Fercovic) y asociados (Dr. Rodrigo Villa-Martínez y Dr. Rodrigo Soteres) gracias por su amabilidad y apoyo incondicional. Hago un especial reconocimiento a mi compañero en las diatomeas, Einer Sepúlveda, quien ha acompañado viajes, terrenos, laburo y dispersión vespertina con la más grata personalidad y con quien fui aprendiendo en paralelo el quehacer diatomístico.

Gran parte de mi motivación ha provenido de mi familia que mediante su sacrificio diario ha hecho posible que pueda perseguir libremente las metas profesionales en curso. Su apoyo también ha sido incondicional. Un especial agradecimiento a mi Madre con quien siempre puedo contar.

Esta tesis fue posible gracias al financiamiento de FONDECYT 1191942, la Iniciativa científica Milenio Núcleo Milenio Paleoclima, el Instituto de Ecología y Biodiversidad (IEB) y el Centro de Ciencia del Clima y la Resiliencia (CR2).

INDEX

LIST OF TABLES

LIST OF FIGURES

ABBREVIATURES

SWW: Southern Westerly Winds; **SH:** Southern hemisphere; **TDPNP:** Torres del Paine National Park; **LC:** Lago Cipreses; **NWP:** Northwestern Patagonia; **SWP:** Southwestern Patagonia; **NWPRFC:** Northwestern Patagonian Rainforest Conifers; **AAP:** Antarctic Peninsula; **EHWDP:** Early Holocene Warm/Dry Period; **LHWDP:** Late Holocene Warm/Dry Period; **IZD:** Interzonal difference; **LDA:** Large-sized diatom assemblage; **PCA:** Principal Component Analysis; **DC:** Diatom cluster; **MC:** Multiproxy cluster; ***PAD*****:** *Planothidium aueri + Achnanthidium spp. cf. mintussimum + Discostella pseudostelligera* assemblage; **DAR:** Diatom accumulation rates; **CHAR:** Charcoal accumulation rates; **NAP:** Non-arboreal pollen; **ka:** calibrated kiloyears before 1950 CE; **OM:** Organic Matter; **IM:** Inorganic Matter; **RoC:** Rates of Change; **LM:** Light microscope; **SEM:** Scanning electron microscope; **SAM:** Southern Annular Mode; **ENSO:** El Niño Southern Oscillation; **SST:** Sea surface temperature

ABSTRACT

A global climate component we faintly understand is the Southern Westerly Winds (SWW). Long-term SWW trends play a major role in determining Southern South American precipitation and fire regimes, deep-sea CO_2 ventilation, Antarctic sea-ice extent, along with energy and moisture transfer between high and low latitudes. SWW behavior is determined by large-scale pressure gradients related to orbital configuration and Earth system circulation patterns. However, on millennial to centennial time scales, key coupled Southern Ocean-atmosphere dynamics are currently blurred by contrasting interpretations regarding SWW evolution during the early Holocene, that ultimately influence how we interpret subsequent periods. Here I present the first continuous diatom record from Southwestern Patagonia (SWP) that spans the entire Holocene, with the intention of contesting contingent hypothesis regarding SWW evolution since the glacial-interglacial transition. The most salient diatom assemblages from Lago Cipreses (51°S) suggest changes in lake freezing and lake mixing regimes, i.e., long and moderate freeze-over seasons occur at times of increased small fragilarioid and *Aulacoseira* abundance, respectively, and turbulent and stratified early-ice off periods occur at times of increased *Aulacoseira* and Non-small fragilarioid benthos abundance, respectively. The results I obtained show the recurrence of environmental conditions reflected in the evolution of the diatom assemblages. In sum with the results of a previously published elemental analysis, pollen, and charcoal record from the same lake, I infer conspicuous warm/dry conditions between ~9-7.4 ka, ~6.1-5.2 ka, and ~3.8-3.1 ka (ka=calibrated kiloyears before 1950 CE), interpreted as weak SWW influence over SWP, and prominent cold/wet conditions between ~14.2–12 ka and ~3.1–0 ka, interpreted as strong SWW influence over SWP. Enhanced hydroclimatic variability is noted to have developed

since ~4 ka. I posit that tropical and extra-tropical climate covariability has evolved throughout the Holocene with variable SWW expressions and suggest that the SWW attained its current position and behavior at ~2.7 ka.

RESUMEN ESPAÑOL

El Cinturón de Vientos del Oeste (CVO) es un componente climático que entendemos vagamente. Tendencias de largo plazo del CVO juegan un rol principal al determinar regímenes de precipitación y de fuego en el Sur de Sudamérica, la ventilación de CO_2 del mar profundo, la extensión de la capa de hielo marino Antárctico y la transferencia de energía y humedad entre latitudes altas y bajas. La naturaleza del CVO está determinada por gradientes de presión de gran escala relacionados con la configuración orbital y patrones de circulación del sistema Terrestre. No obstante, no tenemos un entendimiento acabado de las dinámicas claves del sistema acoplado del Océano Austral-atmósfera debido a interpretaciones contrastantes acerca de la evolución de CVO durante el Holoceno temprano, que afectan la interpretación de periodos subsiguientes. En esta ocasión, presento el primer registro continuo de diatomeas de Patagonia Suroriental (PSO) que abarca todo el Holoceno, con la intención de examinar las hipótesis vigentes sobre la evolución del CVO desde la transición glacial-interglacial. Los ensambles de diatomeas más conspicuos de Lago Cipreses (51°S) sugieren cambios en los regímenes de congelamiento superficial y de mezcla, tales que, periodos largos y moderados de congelamiento superficial ocurren cuando abundan small fragilarioides y *Aulacoseira*, respectivamente, y periodos de turbulencia y estratificación con fecha temprana de derretimiento ocurren cuando abundan *Aulacoseira* y bentos no-small fragilarioide, respectivamente. Los resultados que obtuve muestran la recurrencia de condiciones ambientales que se reflejan en la evolución de los ensambles de diatomeas. En suma, con los resultados del registro de análisis elemental, polen y carbón previamente publicados del mismo lago, infiero condiciones anómalas cálidas/secas entre ~9-7.4 ka, ~6.1-5.2 ka y ~3.8-3.1 (ka=kilo años calibrados antes 1950 e.c.), interpretado

como influencia débil del CVO sobre PSO, y condiciones anómalas frías/húmedas entre ~14.2-12 ka y entre ~3.1-0 ka, atribuible a una fuerte influencia del CVO en la región. Se observa mayor variabilidad hidroclimática desde ~4 ka. Discuto que la covariabilidad entre el clima tropical y extra-tropical ha evolucionado a través del Holoceno con expresiones variadas del CVO y sugiero que la posición y conducta actual del CVO se alcanzó luego de ~2.7 ka.

INTRODUCTION

Motive

The Southern Westerly Winds (SWW), a belt of geostrophic winds that encircles the southern hemisphere (SH) mid-latitudes, are an atmospheric component of pivotal importance in coupled Southern Ocean-atmosphere dynamics with global and local implications. SWW variability has been suggested to regulate atmospheric CO_2 concentration through deep sea upwelling, Antarctic sea-ice extent, SH extratropical climate and fire regimes, and energy and moisture transfer between high and low latitudes (Garreaud, 2007; Garreaud et al., 2009; Hodgson and Sime, 2010; Toggweiler et al., 2006; Toggweiler, 2009; Whitlock et al., 2007). Unfortunately, our understanding of their long-term natural variability is incipient. A better comprehension of centennial to millennial-scale SWW fluctuations in the past is paramount for Earth system dynamics and projections (Fogt and Marshall, 2020; Hodgson and Sime, 2010; Moreno et al., 2018c). Essentially, at glacial-interglacial timescales, poleward SWW migrations can become aligned with the Antarctic Circumpolar Current, in which case throughflow intensity in the Drake Passage is enhanced (Lamy et al., 2015) and CO_2 release from subantarctic mid-depth water is maximized (Toggweiler et al., 2006). Conversely, equatorward-shifted SWW reduce upwelling, degassing of the deep ocean, and energy transfer to the atmosphere and may configure full-glacial conditions passed a certain threshold. Therefore, tracking SWW evolution throughout different time scales is a particularly necessitated endeavor to better understand multimillennial to interdecadal climate variability.

Background

Evidence of synchronous cooling between Antarctica and the SH mid-latitudes during the Antarctic Cold Reversal choronozone (~14.7–13 ka; Pedro et al., 2015) suggests a tight climate coupling at that time (Sagredo et al., 2011; McCulloch et al., 2005; Moreno et al., 2009b, 2012). Antarctic and mid to low latitudes climates, however, seem to decouple as climate warms (Lambert et al., 2008). The SWW may be a key atmospheric component capable of linking climatic changes from SH low and high latitudes (Jara et al., 2015; Pesce and Moreno, 2014). Empirical testing of this hypothesis, however, is precluded by the sparsity of continuous well-constrained paleoclimatic records.

The South American continent extends the farthest south in the SH, and by this merit, exclusively crosses latitudes with peak SWW speeds (Figure 1). Of particular interest is Southwestern Patagonia (SWP; 49°-55°S) that is subject to year-long SWW influence. The SWW drive excess moisture towards the windward side of the Andes, and thus cold/wet conditions in western Patagonia are correlated with strong SWW influence (Garreaud, 2007). Due to this privileged geographic position, paleoclimatic records from this region can track climate-driven landscape changes related to SWW influence.

There is ongoing discussion on whether the SWW migrated poleward, contracted in the core region, or debilitated altogether during the Early Holocene (~11.7–8.2 ka). Records from SWP (~51°S-53°S) strongly diverge in this regard (Heusser, 1995; Kilian and Lamy, 2012; Lamy et al., 2010; Moreno et al., 2010, 2021; Ríos et al., 2020). One set of records, retrieved from diverse depositional environments along fjord systems west of the Strait of Magellan, interpret peak SWW influence over SWP (enhanced precipitation and/or wind strength) during the Early

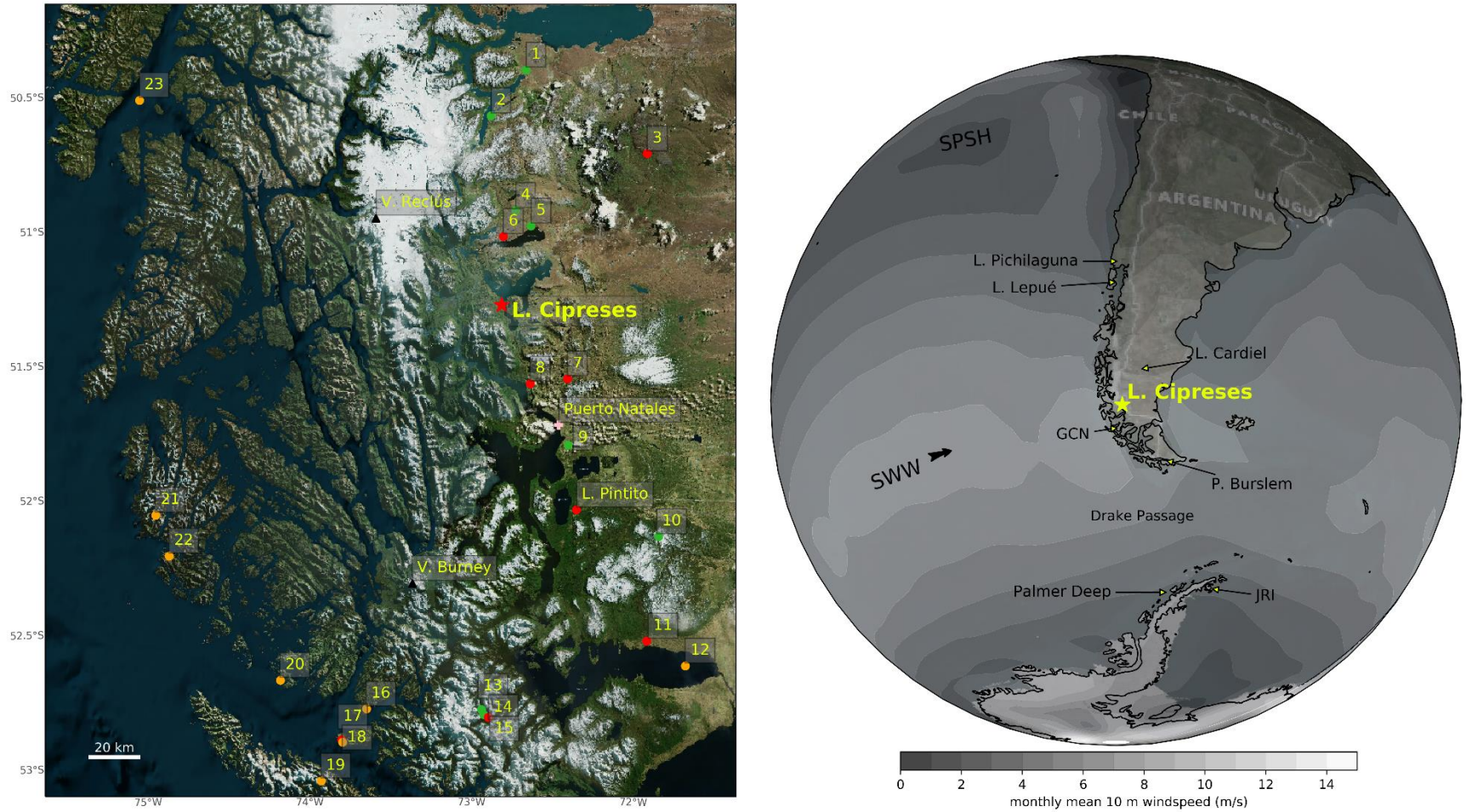

Figure 1. Lago Cipreses (red star) is shown on the left pane along with surrounding lake (red circle), peat (green circle), and marine (orange circle) cores. Volcanoes Reclús and Burney are also shown (black triangle). 1: Cerro Frías; 2: Brazo Sur; 3: L. Las Vizcachas; 4: Vega Ñandú; 5: Torres del Paine; 6: L. Guanaco; 7: L. Dorotea; 8: L. Eberhard; 9: Pantano Dumestre; 10: Río Rubens; 11: L. Escondido; 12: Sk1; 13: GC-1; 14: GC-2; 15: CH-1; 16: Palm2; 17: TML1 (L. Tamar); 18: TM1; 19: Churruca fjord; 20: Par1; 21: Bahía Caribe; 22: Bahía Trampa; 23: MD07-3124. On the right pain: grey-scale contour of the monthly near-surface windspeeds (m/s) averaged between 1979 and 2019 (NCEP/DOE) overlain the southern hemisphere, showing the location of sites discussed throughout this thesis. SWW: Southern Westerly Winds; SPSH: Southern Pacific Subtropical High.

Holocene (Kilian et al., 2007a: Kilian and Lamy, 2012; Lamy et al., 2010). Conversely, an alternative swath of records retrieved from closed-basin lakes and bogs immediately east of the Andean divide infer weak SWW influence in SWP over the same interval (Huber and Markgraf, 2003; Moreno et al., 2010, 2012, 2018c, 2021; Villa-Martínez and Moreno, 2007; Wille and Schäbitz, 2009). Whether anomalously strong or weak SWW presided at the mid-high latitudes during this period has deep ramifications regarding coupled Southern Ocean-atmosphere dynamics in which salient carbon-balance anomalies are implied (Anderson et al., 2009; Hodgson and Sime, 2010; Kilian and Lamy, 2012; Martínez Fontaine et al., 2019; Moreno et al., 2010, 2021; Schmitt et al., 2012).

SWW evolution in SWP during the Middle Holocene (~8.2-4.2 ka) interval is compounded by the mutually exclusive arguments presented for SWW variability during the Early Holocene (Kilian and Lamy, 2012). The heuristic understanding of stronger SWW in the core region during the Early Holocene (Kilian et al., 2007a; Lamy et al., 2010) conveys the picture of a gradual attenuation of SWW influence thereafter, while the converse promotes a sense of SWW reinvigoration, suggested to have occurred by ~7.5 ka (Moreno et al., 2021).

Another dichotomous discussion on whether the SWW had strengthened or abated in the core region circumscribes the Late Holocene interval (~4.2–0 ka). The controversy again evokes opposite poles of SWW expression, namely, reduced (Kilian et al., 2007b; Lamy et al., 2010; Unkel et al., 2010) or enhanced SWW influence in SWP (Moreno et al., 2010, 2018c; Villa-Martínez and Moreno, 2007).

Much of the discrepancy resides in questionable interpretations of SWW influence based on the utilized proxy, depositional environment, and site location relative to the Andean climatic divide.

For example, marine and fjord records have not yet constrained dating imprecisions associated with changing upwelling dynamics throughout the Holocene that may result in varying reservoir age of old carbon (Kilian and Lamy, 2012; Latorre et al., 2017; Martínez Fontaine et al., 2019). Although more attention has been paid to coastline changes throughout the Holocene (Breuer et al., 2013; Kilian et a., 2007a, b; Ríos et al., 2020), the proxy-climate relationship is compounded by the likely imprint of eustatic sea level rise, isostatic rebound, and calving events following the deglacial period (Ríos et al., 2020). On the other hand, pollen records from sites that lie on the leeward side of the Andes have been criticized for being susceptible to the drying effects of foehn winds at times of enhanced SWW circulation, as evaporation may be more important than precipitation in driving vegetation change (Kilian and Lamy, 2012; Lamy et al., 2010). However, the relationship between SWW and positive hydrological balance in these sites was attributed to precipitation spillover as these sites do reside within the area of positively correlated local precipitation and zonal winds (Garreaud et al., 2013; Moy et al., 2008).

Divergent views of SWW evolution in SWP hamper further interrogation of climate change in the SH extra-tropics. A prerequisite to ascertain a coherent chronicle of natural SWW variability with climate system relevance is to resolve SWW evolution in SWP on millennial to centennial scales. Only then can SWW variability in SWP be integrated with indirect evidence of hydroclimatic anomalies north and south of SWP, that hitherto, constrain the subsequent anatomy of multimillennial to centennial-scale SWW fluctuations.

Superimposed on the multimillennial SWW patterns, salient centennial-scale variability has been documented to have emerged sometime between ~6.5 ka and ~4.6 ka in western Patagonia (Fercovic, 2019; Henríquez et al., 2021; McCulloch et al., 2020; Moreno et al., 2018a, 2018c). Although elusive and in the midst of ongoing discussion (Chen et al., 2021; Etourneau et al., 2013;

Fogt and Marshall, 2020; Gomez et al., 2012; Moreno et al., 2018c), modular oceanic and atmospheric centennial-scale circulation patterns, similar to those that account for much of the current interannual and interdecadal climatic variability in the SH extra-tropics (i.e., the Southern Annular Mode [SAM], El Niño Southern Oscillation [ENSO], and Interdecadal Pacific Oscillation [IPO]), have been posited to have developed throughout the Holocene (Gomez et al., 2012; Moreno et al., 2018c; Moy et al., 2002), and may have potentially influenced SWW behavior and propagation of arising teleconnection patterns at centennial scales. Between ~4 ka and ~2.7 ka, a conspicuous cluster of centennial-scale warm/dry anomalies in SWP (Moreno et al., 2018c) and mid-Holocene peak warm conditions in the Antarctic Peninsula (AAP; Kaplan et al., 2020; Mulvaney et al., 2012) coincide with large magnitude N-S fluctuations of the Intertropical Convergence Zone (ITCZ; Haug et al., 2001). Mechanisms involving more energetic SAM-like driven SWW variations through atmospheric wave propagation of augmented ENSO variability, fit proxy and model-based evidence, that may explain co-occurring phenomena such as these (Dätwyler et al., 2020; Moreno et al., 2018c). The next step is to define whether interplay (Gomez et al., 2012), co-dependence (Ding et al., 2012; Etourneau et al, 2013; Fogt and Marshall, 2020), co-variability (Moreno et al., 2018c), or non-stationary spatial expression (Dätwyler et al., 2018; Dätwyler et al., 2020) best explain the relationship between current large-scale modes of climate variability in the past. This requires detailed records of SWW evolution to be coerced by a robust body of empirical evidence.

Diatoms as sensors of past hydroclimatic variations

Lacustrine sedimentary records are invaluable archives of environmental change as they harbor sedimentary and biological signals from the watershed and surroundings, including *in situ* fossil diatom valves. Diatoms have silicified valves with species-specific patterns identifiable through

optical or electronic microscopy. They are microalgae and are essential photosynthetic primary producers in limnic systems. As they have short lifespans, the spawning populations that are most represented in the taxocoenosis of the sediment are those that proliferated the most under the presiding physicochemical/environmental conditions.

These organisms are influenced by limnologic parameters such as temperature, nutrient content and concentration (especially phosphorous, nitrogen, and silica), stratification or mixing regime, pH, photic incidence, ice cover, macrophyte presence, and lake fetch (Smol and Cumming, 2000). Any major changes will be reflected in the dominant diatom assemblage. Although the composition of diatom assemblages is not immune to ash or tephra deposition (Enache and Prairie, 2000; Mayr et al., 2019), their bioindicative potential may accrue an independent line of paleoenvironmental evidence. Additionally, since shifting diatom assemblages may directly reflect various aspects of hydrological fluctuations in the basin, it has been proposed that this proxy may present a higher and more direct sensitivity to hydroclimate variability than changes in vegetation or inorganic markers (Smol and Stoermer, 2010). To this date, however, no continuous diatom record spanning the entire Holocene has been published from the Andean sectors of SWP. Diatom records from this sector would have a stronger relationship with SWW changes, and potentially differ from the evidence accumulated with diatom stratigraphy from Laguna Potrok Aike (Massaferro et al., 2013; Recasens et al., 2015; Wille et al., 2007), which is more adjacent to the Atlantic coast and presents a null-to-negative correlation between surface wind speed and precipitation (Garreaud et al., 2013).

Due to the low coverage of diatom studies in SWP (Díaz Pardo et al., 2008), any paleoclimatic application of these organisms can be considered as a pioneering approach for the region (Fey et al., 2009; Mayr et al., 2019; McCulloch and Davies, 2001). The diversity of diatom species in

stratigraphic studies conducted in SWP has been underestimated by the scarcity of stratigraphic diatom records and broad taxonomical surveys that overlooked local species and variants (Rumrich et al., 2000). More recently, local studies have revealed a rich diversity of unregistered diatom species within the proximity of SWP (García et al., 2018, 2019, 2020, 2021; Guerrero et al., 2019). The optimal conditions, or range of tolerance, for any of the local taxa is only recently being studied and is far from being adequately resolved for developing quantitative environmental reconstructions. This introduces the need for dedicated taxonomical and environmental surveys in SWP, as well as statistical techniques that detect relevant and robust environmental patterns from stratigraphic diatom studies. Multivariate and unsupervised machine learning algorithms could fit this need as they detect covariability patterns occurring throughout the evolution of a large data set. Also, an unbiased assertation of related climate states, and their pace, could be reconstructed if the results are adequately understood within the context of previous evidence.

An eligible paleoenvironmental study that may benefit from diatom-based evidence is that of Moreno et al. (2018c), where they published an elemental analysis, pollen, and charcoal accumulation rates (CHAR) record from a small closed-basin lake in SWP, Lago Cipreses (LC). This site lies in a forested sector on the western slope of Lago del Toro, 10 km southeast of the Torres del Paine National Park (TDPNP) southern border (Figure 1). This study detected warm/dry periods inferred from discrete pulses of non-arboreal pollen (NAP) as they attest to reversible openings in the dominant forest canopy that established in the region and has lingered since ~11 ka. Two clusters of NAP prominent periods were identified: the first between ~10.5 ka and ~7.5 ka was coined the Early Holocene Warm/Dry Period (EHWDP), and the second between ~4 ka and ~2.7 ka was coined the Late Holocene Warm/Dry Period (LHWDP). The former was attributed

to weak SWW in the core region. Furthermore, each centennial-scale NAP pulse was short-named a Cipreses Cycle (CC) and attributed to positive Southern Annular Mode (SAM)-like conditions (warm/dry states) at centennial timescales (more on this in *Regional Setting* section). Additionally, the cold-tolerant hygrophilous conifer *Pilgerodendron uviferum* shows increasing abundance after ~2.7 ka, thus advocating enhanced SWW influence during the Late Holocene.

In this thesis, I present a new high-resolution diatom record from LC to address the following questions: (i) Which environmental factors conditioned the diatom assemblage composition, structure, and changes throughout the Holocene?, (ii) What has been the direction, magnitude, and timing of environmental change in LC?, (iii) Is there evidence for millennial and centennial-scale environmental changes reflected by changes in diatom assemblages over the last 14,000 years?, and (iv) Was the SWW influence maximal or minimal during the early and late Holocene over SWP?

Hypotheses

With respect to the core region of the SWW,

1. If the SWW influence over SWP debilitated between ~10-7.5 ka, then the diatom record from LC should evidence manifestations of warm/dry conditions such as shortened freeze-over seasons during that interval and/or preponderance of low lake levels.
2. If the SWW influence over SWP was superior after ~7.5 ka than before this date, then the LC diatom record should evidence assemblages indicative of ice-free turbulent mixing after and not before that date.

3. If the SWW influence over SWP strengthened after ~3 ka, then the LC diatom record should evidence cold/wet conditions, such as prolonged freeze-over seasons and/or preponderance of higher lake levels, after and not before that date
4. If centennial-scale SWW variability over SWP commenced after ~6.5 ka, then the LC record should exhibit alternation or co-occurrence of diatom assemblages indicative of cold/wet and warm/dry conditions at centennial timescales since that age.

Goal

The general goal of this thesis is to develop a stratigraphic record of variations in diatom assemblages from Lago Cipreses during the Holocene, and infer past environmental changes based on the presence of key indicator assemblages. These results and interpretations constitute independent evidence to test pollen-based environmental interpretations from the same sediment core. Thus, direction, magnitude, and chronology of change can be examined using new independent evidence, benefiting from less reliance on potential -or sensibility to- single-proxy caveats.

After answering the previous questions, I will discuss the following large-scale paleoclimatic aspects in relation to the new results and evidence accrued in neighboring regions as to define SWW dynamics in the past: (i) Did the SWW migrate, strengthen, or debilitate during the Early Holocene? (ii) What is the anatomy and chronology of millennial to centennial-scale SWW change throughout the Holocene? (iii) Do these new results support tropical and extratropical climate covariability throughout the Holocene, and what are the trends herein?

Regional setting

SWP contemplates the Pacific coastal and Andean sectors of South America in the latitudes that span from ~49°S to ~55°S, where the continent is cut off by the Drake Passage in the south (Figure 1). The climate of SWP is highly influenced by the amount and seasonality of westerly precipitation. A steep west to east gradient in precipitation is defined by the presence of the Andean cordillera that promotes orographic rain on the windward side and subsidence of moisture deprived air masses on its leeward side (Garreaud et al., 2013). Climatologic studies have detected a significant correlation between near-surface (850 hPa) wind speeds and the amount of local precipitation, which is positive and significant west of the Andes and turns negative east of the Andes under a pronounced rain shadow effect (Garreaud, 2007; Schneider et al., 2003). Nonetheless, spillover of moist air masses across the Andes maintains positive correlations in sectors located 50 to 70 km east of the Andean divide (Moreno et al., 2018c). The distribution of vegetation reflects this gradient with Magellanic Moorland vegetation on the western hyperhumid maritime sectors, grading eastwards with the occupation of Evergreen forests, followed by deciduous forests, and finally, the Patagonian steppe that extends to the Atlantic coast (Pisano, 1992). High Andean vegetation above the timberline attests to colder/wetter conditions that transition downslope to mixed deciduous-evergreen forests and then to xeric Patagonian steppe as temperature rises and precipitation declines with decreasing altitude toward the east. Glaciers and extensive ice fields (*Campo de Hielo Sur*/South Patagonian Icefield) also attest to these gradients as they are situated on the uppermost humid sectors of the Andean range.

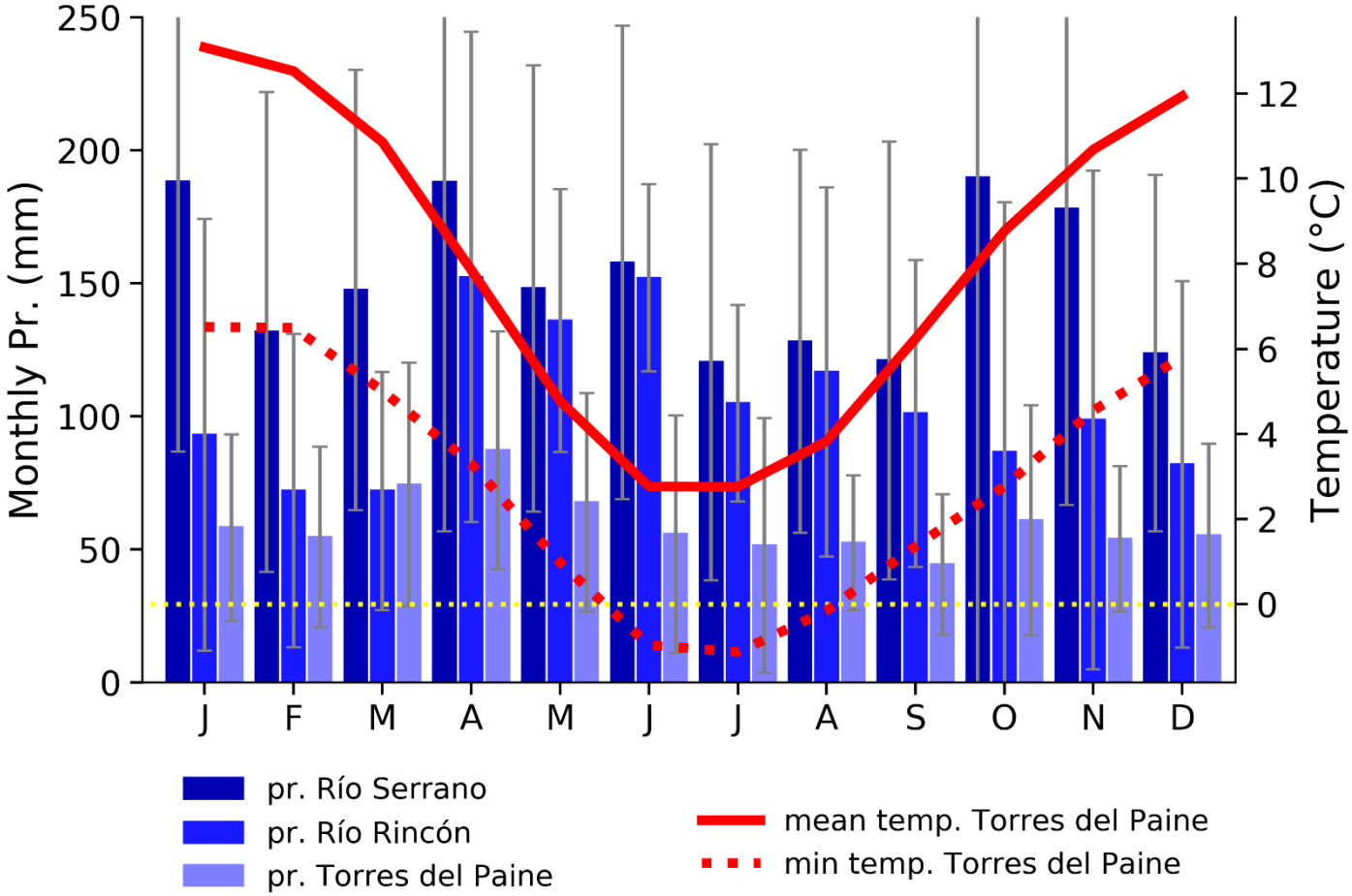

Figure 2. Monthly temperature and precipitation from nearby weather stations provided by the CR2 explorer. Mean monthly temperature is drawn in the continuous red line, mean monthly minimum temperature in dotted red line, and blue bars present monthly precipitation from the indicated weather station, along with standard deviations.

The climatology of SWP is intimately related with the synoptic dynamics of the SWW. During the austral summer season (DJF), the SWW contract towards the core region between ~48° and 52°S, resulting in increased wind speed and precipitation in SWP. The interpolated average temperature over LC during this season is 11.7°C with an average maximum (minimum) of 16.2°C (7.4°C), along with a mean monthly precipitation of 38.8 mm and a monthly maximum (minimum) of 68.8 mm (17.7 mm), calculated between 1979 and 2016 (Boiser et al., 2018). During the austral winter season (JJA), the South Pacific Subtropical High weakens, and the SWW expand northwards, reaching as far north as 30°S, in which case segregated fronts branch off the storm tracks. In the process of expansion, winds weaken over the core region, delivering lower rainfall. The average temperature in this season is 3.1°C with an average maximum (minimum) of 6.4°C (-0.4°C), along with a mean monthly precipitation of 43.3 mm and a monthly maximum (minimum) of 78.9 mm (19.3 mm), recorded between 1979 and 2016 (Boiser et al., 2018). The calculated annual precipitation is 610 mm. Figure 2 shows observational data from nearby weather stations. It may be noted that temperature significantly decreases during winter months, while different weather stations present distinct annual pluvial regimes. The Río Rincón station (~6 km south-southeast from LC) is the closest and features the highest rainfall between April and July, while the Río Serrano station (~18 km west-southwest from LC) features the highest rainfall in January, April, October, and November.

Interannual variability in SWP is governed by the polarity of the Southern Annular Mode (SAM). This index measures the global difference of sea level pressure anomalies between mid (~40°S) and high latitudes (~65°S) (Gong and Wang, 1999). Anomalous high pressure over the mid-latitudes indicates a presiding positive SAM phase in which SWW are deflected poleward. Conversely, a negative SAM phase is registered when high pressures over the high latitudes

deflect the SWW northwards. Mid-latitude landmasses influenced by this mode of variability (e.g., New Zealand, Tasmania, SWP) experience less (more) precipitation and higher (lower) temperatures during positive (negative) phases (Garreaud et al., 2009). Although El Niño Southern Oscillation (ENSO) influences large parts of the world, climate anomalies in SWP show little correlation with ENSO variability (Aravena and Luckman, 2009; Garreaud et al., 2009; Schneider and Gies, 2004).

Site description

This study is based on sediment cores retrieved from LC, a small bedrock-basin lake (51.285°S, 72.854°W; Figure 1), located south of TDPNP on the eastern foothills of Cordillera Arturo Prat, a segment of the austral Andes separated from the main cordillera by the narrow, <8 km wide, Última Esperanza fjord. LC lies adjacent to Lago del Toro at an elevation of 110 masl. The lake has a maximum water depth of 8.4 m. During the winter season, the lake is known to freeze over. No permanent inlets or outlets are present, although a small ravine along its western sector supplies seasonal snow-melt discharge, and a sill ~1 m above the current lake surface on its eastern sector may act as a spillway at times of higher lake level. LC lies between the hyper humid Southern Patagonian Icefield to the west and the xeric Patagonian steppe to the east; nested atop a forested slope between interconnected basins that drain to the Pacific Ocean through Río Prat immediately downslope to the east and proglacial lakes that drain to the Última Esperanza fjord through Río Serrano to the west.

Glacier lobes originated from the Patagonian Ice Sheet and flowed southward from TDPNP into Lago del Toro, and northward from Seno Última Esperanza (SUE) into the Lago Porteño sector during the Last Glacial Maximum (~25–18 ka) (Marden, 1997; *cf.* Sagredo et al., 2011). Glacier

recession during the last glacial termination exposed an ice-molded landscape and dammed a large proglacial lake in SUE and adjacent sectors. A sequence of glaciolacustrine regressive pulses occurred between ~16.3 ka and 11 ka that led to individualization of LC as a closed-basin lake. The sector nearest to LC was colonized by pioneer cold-tolerant herbs and shrubs, followed by a rapid spread of trees of the genus *Nothofagus*, woodland encroachment, and ultimately the establishment of closed-canopy forests by ~11 ka (Moreno et al., 2018c). As previously mentioned, intermittent and reversible increments in NAP revealed in the LC pollen record suggests periods of canopy aperture throughout the Holocene, which are prominently clustered between ~10.5-7.5 ka and ~4.1–2.7 ka.

MATERIALS AND METHODS

I recovered a diatom record from sediment cores (PS0710SC1+PS0710AT1+PS0710AT2+ PS0710AT3) extracted from the deepest sector of LC in 2007 (Moreno et al., 2018c). The diatom analyses are based on 1-cc sediment samples obtained from every other cm between 1 and 282 cm, and from continuous/contiguous samples from every centimeter between 282 and 322 cm. I applied standard methods to process and digest each sample (Batterbee, 1986) which involve H_20_2 and H_2SO_4 to remove the organic matter content of the sediments. Some samples that did not react sufficiently to this treatment were subjected to a stronger oxidative treatment with $KMnO_4$ and H_2O_2 (Hasle and Fryxell, 1970). I mounted all samples on Light Microscope (LM) slides with Naphrax® and placed aliquots of selected samples to dry on aluminum stubs for a gold coating (20 nm thickness), as they were destined for Electron Scanning Microscope (SEM) observations.

I performed LM observations at the Laboratorio de Diatomeas Continentales (Universidad de Buenos Aires, Argentina) with a Polyvar Reichert-Jung binocular LM equipped with a Plan Apo 100x, NA 1.32, immersion objective, DIC optics, and a Canon EOS 600D camera. I performed SEM observations with a Carl Zeiss SUPRA 40 (15kv) at the Centro de Microscopías Avanzadas (CMA; FCEN, Universidad de Buenos Aires, Argentina). I considered any pertinent taxonomic literature, with special emphasis on publications with a regional focus (García et al., 2019, 2021; Hofmann et al., 2011; Kramer, 1991, 1997, 2000, 2003; Kramer and Lange-Bertalot, 1986, 1988; Lange-Bertalot, 1994,1996, 2001; Lange-Bertalot and Kramer, 1989; Lange-Bertalot et al., 2011; Mann

et al., 2004; Reichardt, 2015; Rumrich, 2000; Sala and Ramírez, 2008; Van de Vijver et al., 2002, 2004; Wetzel et al., 2015).

I obtained qualitative and quantitative diatom data by recording the number of slide-transverses completed after counting a minimum of 300 valves with the 100x objective (1000x total magnification). I then calculated the concentration of diatoms in a gram of sediment with Equation 1,

Equation 1: $$\frac{\frac{V_i}{2} cells * \frac{T_t}{T_i} * D_i}{M_i\, g} = Diatom\ cells/g$$

where V_i is the number of valves, T_i is the counted transverses with respect to total transverses on a slide (T_t), D_i is the dilution factor, and M_i is the dry weight of 1 cc of sediment in sample i (Schrader and Gersonde, 1978). I recalibrated the age-depth model presented in Moreno et al. (2018c) with SHcal20 (Hogg et al., 2020) using the R Bacon package (Blaaw and Christen, 2013) and used this age-depth model for the stratigraphy of this study (Figure S1). To obtain flux or diatom accumulation rates (DAR), I standardized the concentration of each sample by the depositional time, according to the age-depth model.

I summarized the broad tendencies of the data I collected from diatom assemblages as functional groups. I considered the following functional groups as suitable for the composition found in this record: plankton, *Aulacoseira*, small fragilarioids and non-small fragilarioid benthos (NFB). A complete binary listing of functional group assignation can be found in Table SI.

I performed a suite of statistical analysis on the diatom counts, including a stratigraphically constrained hierarchical cluster analysis (CONISS method; Grimm, 1987) applied to a Bray-Curtis dissimilarity matrix resulting from the relative abundance data using the R rioja package (v0.9-

26; Juggins and Juggins, 2020). Secondly, I applied a Principal Component Analysis (PCA; Filzmoser and Todorov, 2013) to a database with the z-score (variance standardization) of 7 of the most abundant taxa recorded using scikit-learn (v0.23.1) in Python (v3.8.3). Third, I developed a k-means cluster analysis (3 clusters; 100 iterations of k++ initiations) with the small fragilarioid and *Aulacoseira* groups using scikit-learn (v0.23.1) in Python (v3.8.3). Fourth, I performed a Rates of Changes (RoC) analysis using the R-ratepol R package (Mottl et al., 2021) using the Grimm smoothing method with 5 shifts, 60-year interpolations, and chord distance matrix. I obtained significant peak points using a non-linear trend model. I repeated and expanded this PCA/k-means (4 cluster) pipeline with the diatom functional groups and the loss of ignition (LOI), elemental analysis, pollen, macroscopic charcoal accumulation rates (CHAR) database from the same sedimentary core (Moreno et al., 2018c) to obtain the statistically supported recurrence of environmental conditions through the multiproxy integration.

RESULTS

Diatom characterization and stratigraphy

I identified 158 infrageneric diatom taxa from 179 levels that span the last ~14,200 years in the sediment core from LC, with a median time resolution of 71 years between levels. Further analysis with SEM aided the identification of taxa with submicroscopic diagnostic features as well as a species new to science, *Pseudostaurosira australopatagonica* M.L. García, L.A. Villacís, Maidana & E. Morales, which we published recently (García et al., 2021). I grouped all small fragilarioids, as they require SEM resolution to distinguish between species. For counting purposes, I also grouped *Aulacoseira humilis* with *Aulacoseira liucoensis*, referred to as *Aulacoseira humilis/liucoensis*. Figure 3 features these species, where it may be noted that specimens of *A. humisis* (a1 and a2) and *A. liucoensis* (b1 and b2) are indistinguishable when seen in girdle view with LM. Only SEM images (a3 and b4) or a valve view in LM (A4 and B4) permits a taxonomic distinguishment between species.

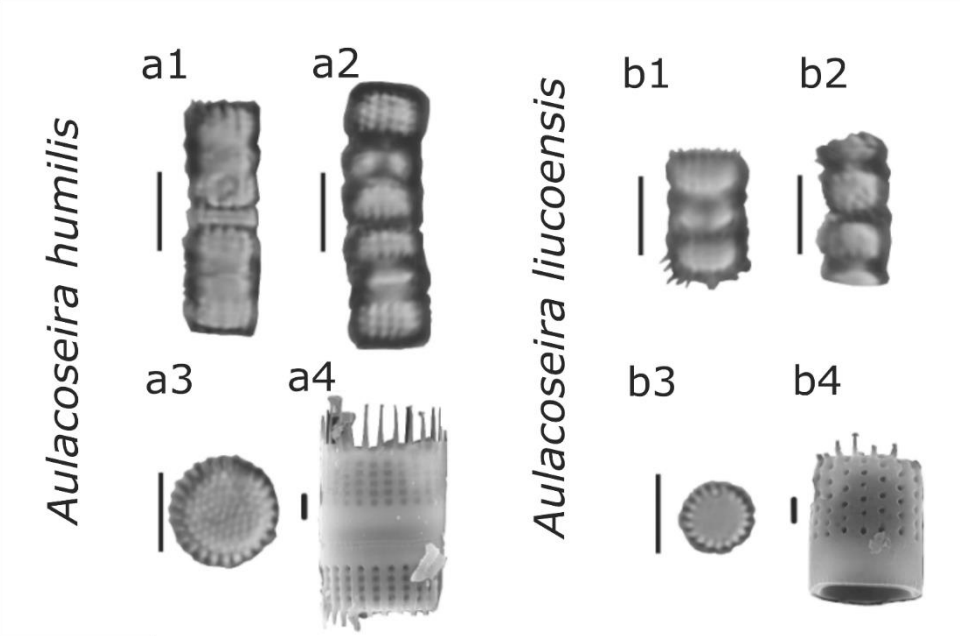

Figure 3. a1-a4: *Aulacoseira humilis*. a1-a2 (LM), A4 (SEM) girdle views. a3 (LM) valve view. Notice areolae pattern on valve face in a3. b1-b4: *Aulacoseira liucoensis*. b1-b2 (LM) and b4 (SEM) girdle views, b3 (LM) valve views. Notice the absence of areolae in b3. Black bar in a1, a2, a3, b1, b2, and b3 = 5 µm. Black bar in a4 and b4 = 1 µm.

With the aforementioned groupings, I sequentially split the resulting diatom record into 10 zones (CIP-1 through CIP-10), as determined by a detailed assessment of the evolving diatom assemblages and supported by the CONISS hierarchical clustering method. The following is the characterization of each zone as represented by the taxa with the highest mean abundance values (Figure 4). The interzonal difference (IZD) is the difference between mean abundance values of the present and former zone.

Zone CIP-1 Small fragilarioids-*Denticula kuetzingii-Adlafia sp.* (321-310.5 cm depth, 10 levels, ~14.2–12 ka). The basal zone features an assemblage dominated by small fragilarioids (mean: 69.2%), also containing the record-wide maxima (97.2%) for this group, which is interrupted by

an important increment of the benthic species *Denticola kuetzingii* (mean: 8.3%, max: 23.5%) and *Adlafia sp.* (mean: 6.3%, max: 42.3%) .

Zone CIP-2 *Aulacoseira humilis/liucoensis*–small fragilarioids-*Discostella pseudostelligera* (310.5-294.5 cm depth, 16 levels, ~12–10.4 ka). This zone features a step-wise transition towards an assemblage composed of *Aulacoseira humilis/liucoensis* (mean: 19.5%, max: 65.2%, IZD= +19.4%) and *Aulacoseira lauquenensis* (mean: 4.4%, max: 10.8%, IZD= +4.4%), and the planktonic *Discostella pseudostelligera* (mean: 9.8%, max: 33.1%, IZD: +8.8%). The appearance of *D. pseudostelligera* is followed by *A. humilis/liucoensis* through sequential unimodal patterns of ascent and descent. These changes are accompanied by a 54.9% mean decrease of previously dominant small fragilarioids. Nonetheless, the small fragilarioid group maintains a relatively low abundance during the entire zone (mean: 14.2%). *Adlafia sp.* (mean: 0.4%, IZD: -6.0%) virtually disappears and *Denticola kuetzingii* (mean: 7.5%, IZD: -0.7%) maintains a similar mean abundance with respect to CIP-1, although showing a negative trend throughout this zone.

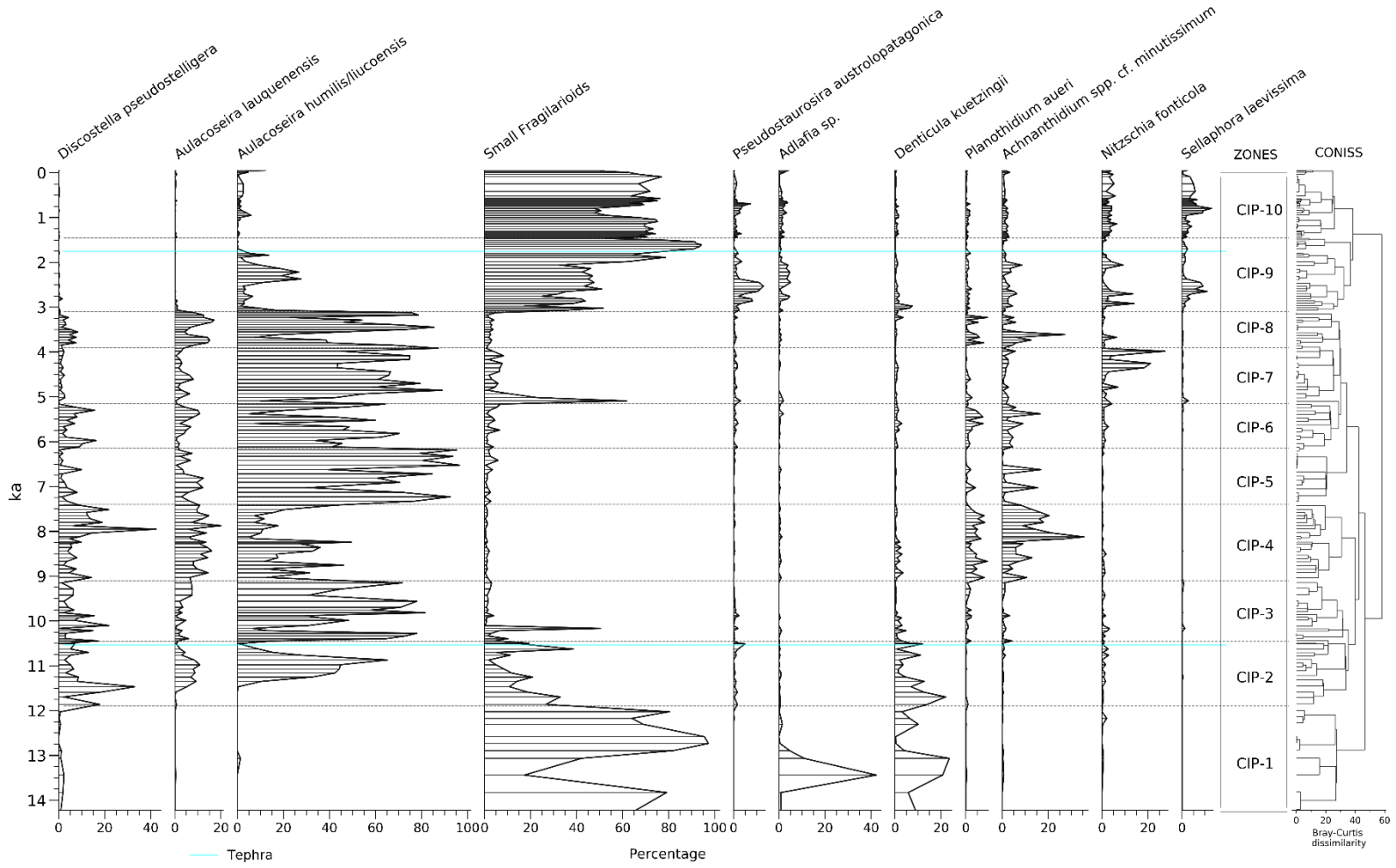

Figure 4. Percentage diagram of the most abundant diatoms. Shown is an age scale in calibrated kiloyears before 1950 CE, along with zones and CONISS method analysis, making use of Bray-Curtis dissimilarity for hierarchical clustering. Tephra positions are shown in cyan shading.

Zone CIP-3 *Aulacoseira humilis/liucoensis–Discostella pseudostelligera*–small fragilarioids (294.5–273 cm depth, 16 levels, ~10.4–9.1 ka). *Aulacoseira humilis/liucoensis* (mean: 51.0%, max=81.5%, IZD: +31.5%) shows a sharp increase that culminates in a sustained peak of ~70% abundance, albeit presenting high variability (σ=23.5%) throughout the zone. *Discostella pseudostelligera* abundance remains relatively low (mean: 6.6%, IZD: -3.1%), however surpassing the small fragilarioid presence as these taxa reach trace abundance (mean: 4.9%, IZD: -9.3%) following an early increment in one level (~10.1 ka); this occurs during a brief window of low *A. humilis/liucoensis* abundance. The benthic species *Denticula kuetzingii* also diminishes significantly (mean: 1.1%, IZD: -6.5%).

Zone CIP-4 *Aulacoseira humilis/liucoensis–Achnanthidium spp. cf. minutissimum–Aulacoseira lauquenensis–Discostella pseudostelligera* (273–231 cm depth, 22 levels, ~9.1–7.4 ka). This zone features a near synchronous increase of *Achnanthidium spp. cf. minutissimum* (mean= 12.1%, max= 35.5%, IZD= +11.3%), *Aulacoseira lauquenensis* (mean= 11.0%, max= 20.1%, IZD= +7.8%), the planktonic *Discostella pseudostelligera* (mean= 10.7%, max= 42.4%, IZD= +4.0%), and *Planothidium aueri* (mean: 4.4%, max: 9.3%, IZD: 3.5%) coeval with the plummeting abundance of *Aulacoseira humilis/liucoensis* (mean= 20.5%, max= 49.5%, IZD= -30.5%). *Achnanthidium spp. cf. minutissimum* and *D. pseudostelligera* feature a positive trend that is antiphase with the negative trend of *Aulacoseira humilis/liucoenisis.*

Zone CIP-5 *Aulacoseira humilis/liucoensis–Aulacoseira lauquenensis–Achnanthidium spp. cf. mintussimum* (231–205 cm depth, 13 levels, ~7.4–6.1 ka). This zone commences with a sharp increment of *Aulacoseira humilis/liucoensis* (mean= 74.8%, max= 96.5%, IZD= +54.3%) which evolves towards a sustained global maximum towards the roof of this zone. The second highest mean abundance corresponds to *Aulacoseira lauquenensis* (mean= 5.8%, IZD= -5.3%) with a

zonal maximum of 12.3%. *Achnanthidium spp. cf. mintussimum* (mean: 3.0%; IZD: -9.1%), *Discostella pseudostelligera* (mean: 2.8%; IZD: -7.9%), and *Planothidium aueri* (mean: 0.7%; IZD: -3.7%) feature important decreases, exceptionally rising at the expense of two sharp declines of *Aulacoseira humilis/liucoensis* at ~7 ka and ~6.6 ka.

Zone CIP-6 *Aulacoseira humilis/liucoensis–Discostella pseudostelligera–Achnanthidium spp. cf. mintussimum* (205–177 cm depth, 14 levels, ~6.1–5.1 ka). The abundance of *Aulacoseira humilis/liucoensis* undergoes variable large-magnitude decreases (mean= 42.5%, max= 70.4%, IZD= -32.3%, σ=19.2%). Levels with low abundance of *Aulacoseira humilis/liucoensis* feature increases of *Discostella pseudostelligera* (mean= 6.8%, max= 16.4%, IZD= +4.0%), *Achnanthidium spp. cf. mintussimum* (mean= 4.8%, max= 16.6%, IZD= +1.8%), and *Planothidium aueri* (mean= 2.8%, max= 7.6%, IZD= +2.1%).

Zone CIP-7 *Aulacoseira humilis/liucoensis*-small fragilarioids-*Nitzschia fonticola* (177–147 cm depth, 15 levels, ~5.1–3.9 ka). *A. humilis/liucoensis* recovers peak abundance (mean= 59.9%, max= 89.0%, IZD= +17.4%) after a gradual rise that is interrupted by peak of small fragilarioid abundance (mean= 8.9%, max= 58.7%, IZD= +6.7%) near the base of the zone (~5 ka). The benthic species *Nitzschia fonticola* (mean= 6.3%, max= 27.4%, IZD= +4.9%) experiences a conspicuous increase towards the roof of the zone. *Achnanthidium spp. cf. mintussimum* (mean: 1.8%, IZD: -3.0%), *Discostella pseudostelligera* (mean: 1.5%, IZD: -5.3%), and *Planothidium aueri* (mean: 0.6%, IZD: -2.2%) again feature an important decrease.

Zone CIP-8 *Aulacoseira humilis/liucoensis-Aulacoseira lauquenensis-Achnanthidium spp. cf. mintussimum* (147–119 cm depth, 14 levels, ~3.9–3.1 ka). This zone features a reversal to a composition and abundance distribution similar to CIP-6 and CIP-4. While *Aulacoseira*

humilis/liucoensis (mean= 51.5%, max= 85.4%, IZD= -8.4%) declines in two occasions, *Aulacoseira lauquenensis* (mean= 10.8%, max= 17.1%, IZD= +7.7%), *Achnanthidium spp. cf. mintussimum* (mean= 5.5%, max= 27.2%, IZD= +3.7%), *Discostella pseudostelligera* (mean= 3.8%, max= 8.3%, IZD= +2.4%), and *Planothidium aueri* (mean= 2.7%, max= 9.3%, IZD= +2.2%) feature corresponding increases.

Zone CIP-9 Small fragilarioids-*Aulacoseira humilis/liucoensis-Pseudostaurosira australopatagonica* (119–64 cm depth, 28 levels, ~3.1–1.4 ka). This zone features an abrupt compositional transition corroborated by the CONISS based analysis as the bifurcation with the highest Bray-Curtis dissimilarity value (57.5). Previously important species virtually disappear (i.e., *Discostella pseudostelligera*¸ mean= 0.1%, IZD= -3.7%; *Aulacoseira lauquenensis*, mean= 0.2%, IZD= -10.6%) or become secondary (i.e., *Aulacoseira humilis/liucoensis*, mean= 6.9%, max= 27.7%, IZD= -44.6%; *Achnanthidium spp. cf. mintussimum*, mean= 2.2%, max= 8.5%, IZD= -3.3%; *Planothidium aueri*, mean= 0.8%, max= 2.5%, IZD= -2.0%). In their place, small fragilarioids (mean: 51.7%, max: 94.1%, IZD: +49.6%) abruptly surge and dominate with a positive trend that culminates at ~92% abundance between ~1.7-1.5 ka. The benthic species *Sellaphora laevissima* (mean= 2.3%;, IZD= +2.2%), *Nitzschia fonticola* (mean= 2.6%, IZD= +2.2%), and *Adlafia sp.* (mean= 1.7%, IZD= +1.4%) also feature notable increments. The recently described small fragilarioid species *Pseudostaurosira australopatagonica* (mean= 3.4%, max: 13.0%, IZD= +2.9%) shows its highest abundance in this zone.

Zone CIP-10 Small fragilarioids-*Sellaphora laevissima-Nitzschia fonticola* (64–1 cm depth, 31 levels, ~1.4 ka – 2002 CE) is principally composed of small fragilarioids (mean= 64.3%, IZD= +12.6%) that attain a higher mean abundance than CIP-9. Nonetheless, increments of *Sellaphora laevissima* (mean= 3.9%, IZD= +1.5%) and *Pseudostaurosira australopatagonica* (mean= 1.6%,

IZD= -1.8%) punctuate the small fragilarioid dominance between ~0.9-0.7 ka. *Aulacoseira humilis/liucoensis* (mean= 1.8%, IZD= -5.1%) maintains a low abundance throughout this zone, albeit a moderate peak in the last level (max= 12.3%).

Principal Component Analysis

A principal component analysis (PCA) derived from 7 selected taxa resulted in a first and second principal component that accounts for 44.1% and 24.4% of the total variance, respectively (Figure 5; Table I). Positive loadings for the first component (PC1) correspond to *Aulacoseira lauquenensis* (0.45), *Planothidium aueri* (0.37), *Discostella pseudostelligera* (0.36), *Achnanthidium spp. cf. minutissimum* (0.34), and *Aulacoseira humilis/liucoensis* (0.24), while negative loadings correspond to small fragilarioids (-0.49) and *Sellaphora laevissima* (-0.39). Regarding the second principal component (PC2), positive loadings correspond to *Achnanthidium spp. cf. minutissimum* (0.46), *Planothidium aueri* (0.44), *Sellaphora laevissima* (0.29), small fragilarioids (0.27) and *Discostella pseudostelligera* (0.19), while negative loadings correspond to *Aulacoseira humilis/liucoensis* (-0.63) and *Aulacoseira lauquenensis* (-0.03)

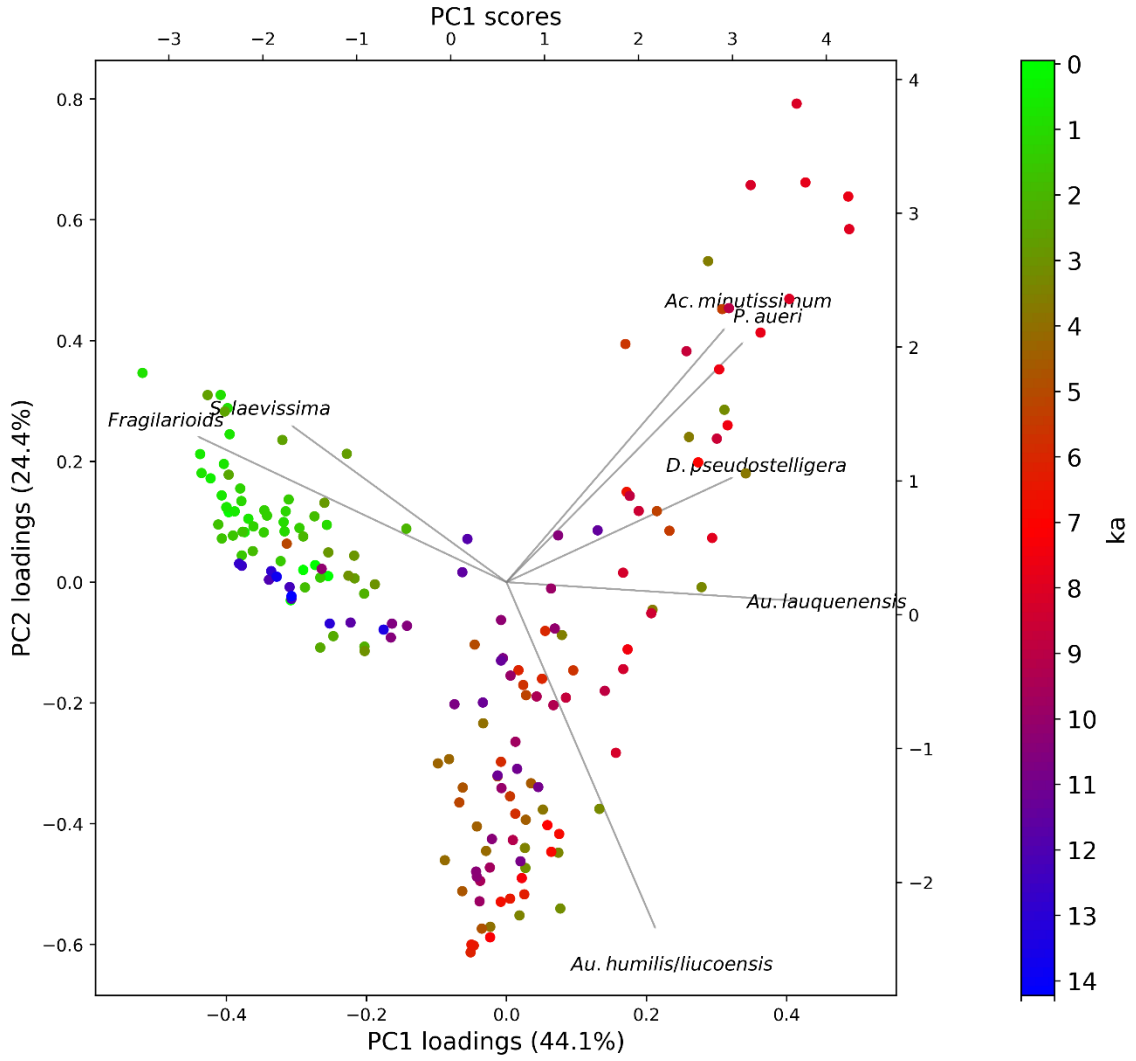

Figure 5. Biplot of principal component analysis applied to the most abundant diatoms. The color of each observational level (dots) corresponds to the date shown by the color bar to the right.

Table I Loadings of diatom PCA

Component	Variance explained	Positive	Negative
PC1	44.1%	*Aulacoseira lauquenensis:* **0.45** *Planothidium aueri*: **0.37** *Discostella pseudostelligera*: **0.36** *Achnanthidium spp. cf. minutissimum*: **0.34** *Aulacoseira humilis/liucoenis*: **0.24**	Small fragilarioids: **-0.49** *Sellaphora laevissima*: **-0.39**
PC2	24.4%	*Achnanthidium spp. cf. minutissimum*: **0.46** *Planothidium aueri*: **0.44** *Sellaphora laevissima*: **0.29** Small fragilarioids: **0.27** *Discostella pseudostelligera*: **0.19**	*Aulacoseira humilis/liucoensis*: **-0.63** *Aulacoseira lauquenensis*: **-0.03**

The evolution of PC1 (Figure 6.a) features strong negative deviations between ~14.2-11.5 ka, followed by positive deviations until ~3.1 ka, with the strongest positive deviations between ~9.1-7.4 ka, ~5.6-5.3 ka, and ~3.8-3.1 ka. This interval is punctuated by strong negative deviations at ~10.1 ka and ~5 ka. A strong negative trend persists for the remainder of the record (~3.1-0 ka) with a notable reversal to near-mean values between ~2.2-2 ka. The PC2 time series (Figure 6.b) features near-mean values between ~14.2-11.2 ka, at which point strong negative to near-mean values last until ~2.7 ka, punctuated by strong positive deviations at ~9 ka, ~8.6 ka, ~8.1-7.5 ka, ~5.6 ka, ~5.3 ka and ~3.6 ka. Positive values persist afterwards (~2.7-0 ka), with a notable reversal to near-mean values between ~2.3-2.1 ka.

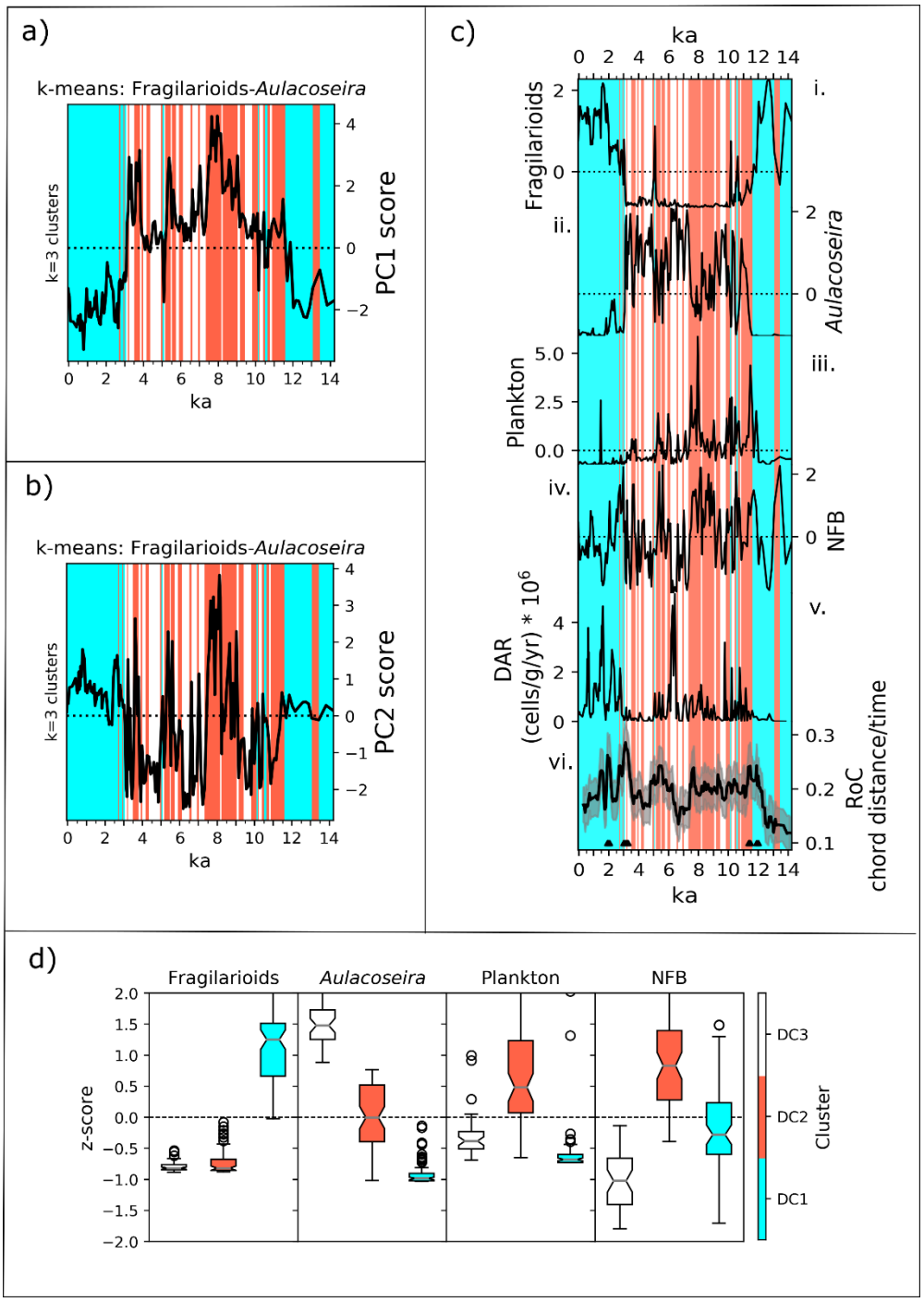

Figure 6. a) diatom PC1 time series over 3-cluster k-means analysis backdrop derived from *Aulacoseira* and small fragilarioid series. b) same as a) but with diatom PC2 time series. c) Time series of small fragilarioids (i), *Aulacoseira* (ii), plankton (iii), NFB (iv) groups, along with DAR (v) and RoC (vi) curves. Black triangles under the RoC curve represent detected significant peak points. d) box plots of each group relating to each diatom cluster (DC).

Functional grouping

I assigned all the taxa in this study to one of four groups: small fragilarioids, *Aulacoseira,* plankton, and non-small fragilarioid benthos (NFB), whose percentual sum was then standardized to enable the detection of statistical anomalies. The small fragilarioid group shows strong positive deviations between ~14.2-12 ka, that transition to a sustained negative deviation between ~10.1-3.1 ka, which is then followed by a sharp transition to positive deviations (Figure 6.c.i). A strong positive deviation at ~5 ka punctuates the interval of negative deviations. The *Aulacoseira* group features negative deviations in the oldest and youngest portions of the record, separated by an interval of prominent positive deviations bracketed between ~11.2-3.1 ka, punctuated by negative deviations at ~10.6-10.4 ka, ~9-8.5 ka, ~8.1-7.5 ka, ~5.6 ka, ~5 ka, and ~3.6 ka (Figure 6.c.ii). The plankton group features sharp positive deviations at ~11.8-11.4 ka, ~10.7-10.4 ka, ~10.2-9.8 ka, ~9 ka, ~8.2-7.4 ka, ~6 ka, ~5.3 ka, and ~1.4 ka (Figure 6.c.iii). Lastly, the NFB time series features a highly variable evolution with prominent positive deviations at ~13.4-13 ka, ~11.8-11.3 ka, ~10.7-10.4 ka, ~10.2-9.8 ka, ~9-7.5 ka, ~5.6 ka, ~5.3 ka, ~3.6 ka, ~3.2 ka, ~2.9-2.5 ka, ~2 ka, and ~0.9-0.7 ka (Figure 6.c.iv).

k-means analysis

I used the small fragilarioid and *Aulacoseira* groups to generate a k-means analysis with three clusters in order to statistically detect recurring diatom assemblages throughout the record (Figure 6.a and 6.b). The first diatom cluster (DC1; cyan) is associated with high small fragilarioid abundance (Figure 6.d) and was assigned to the following sections: ~14.2-13.8 ka, ~13-11.7 ka, ~10.6 ka, ~10.1 ka, ~5 ka, and ~3-0 ka. The second diatom cluster (DC2; red) is associated with high plankton and NFB abundance and was assigned to the following sections: ~13.4 ka, ~11.6-

10.7 ka, ~10.5 ka, ~10.1-9.8 ka, ~9.4-7.4 ka, ~7 ka, ~6.6 ka, ~6.1-6 ka, ~5.7-5.2 ka, ~4.3 ka, ~4 ka, ~3.8-3.5 ka, ~3.2 ka, ~3 ka, and ~2.7 ka. The third diatom cluster (DC3; white) alternates with DC2, is associated with high *Aulacoseira* abundance, and was most prominently assigned between ~10.4-10.3 ka, ~9.8-9.5 ka, ~7.3-6.2 ka, ~4.9-4.4 ka, ~3.5-3.1 ka.

Diatom accumulation rates

I calculated the diatom accumulation rate (DAR) for each level that resulted in a mean of $0.3*10^6$ cells/g/year, a median of $0.7*10^6$ cells/g/year, and a standard deviation of $1.0*10^6$ cells/g/year. The time series (Figure 6.c.v) features low values during the initial part of the record, followed by a variable positive trend between ~11.6-9.7 ka, culminating with a value of $3.2*10^6$ cells/g/year. Subsequently, DAR values decrease and then oscillate between ~9-5 ka with a median of $0.4*10^6$ cells/g/year, with a pronounced peak that reaches a maxima of $5.2*10^6$ cells/y/gr at ~6.4-6.1 ka. Between ~5-2.9 ka, DAR values drop to a median of $0.1*10^6$ cells/g/year, and then increase significantly after ~2.8 ka, featuring a median value of $1.0*10^6$ cells/g/year until present. During this last interval DAR values reach as high as $4.7*10^6$ cells/g/yr.

Rates of change

I calculated the rates of change (RoC) parameter from the diatom abundance data. RoC values describe the magnitude diatom assemblage change throughout the record (Figure 6.c.vi). The initial portion of the record shows a positive trend, commencing with the lowest values in the record and culminating with an interval of significantly abrupt changes (high values) between ~12-11.3 ka. Subsequently, values remain relatively high until ~7.4 ka, at which point values decrease until ~6.3 ka. Values then increase between ~6.2-4.8 ka, decrease between ~4.7-3.5 ka,

and at ~3.3-3 ka increase to significantly high values. The remainder of the record features a negative trend with a significant reversal at ~2-1.9 ka.

Multiproxy analysis

Moreno et al. (2018c) presented a complete loss of ignition (LOI), elemental analysis, pollen, and macroscopic charcoal accumulation rates (CHAR) record from LC. With this data I generated a multiproxy analysis that includes a PCA and k-means clustering. The purpose of incorporating other proxies is to statistically integrate diatom-based limnological changes with the surrounding terrestrial changes described in Moreno et al. (2018c).

Multiproxy principal component analysis

I used the following variables to generate a multiproxy PCA: % inorganic matter (IM), % calcium carbonate ($CaCO_3$), % organic matter (OM), the ratio of atomic carbon and nitrogen (C/N), % small fragilarioids, % *Aulacoseira,* % plankton, % NFB, CHAR, % arboreal pollen (Trees), % *Pilgerodendron uviferum*, % non-arboreal pollen (NAP), % ferns, and % aquatic pollen, spores, and green algae (aquatics). The resulting multiproxy PCA (Figure 7) features a first and second principal component that accounts for 35.3% and 16.5% of the total variance, respectively (Figure 7; Table II). Positive loadings for the first component (multiproxy PC1) correspond mainly to NAP (0.42), IM (0.39), ferns (0.37), and aquatics (0.32), while negative loadings correspond mainly to trees (-0.42), OM (-0.39) and C/N (-0.24). Regarding the second principal component (multiproxy PC2), positive loadings correspond mainly to small fragilarioids (0.61) and *P. uviferum* (0.28), while negative loadings correspond mainly to *Aulacoseira* (-0.42), plankton (-0.38), and C/N (-0.31).

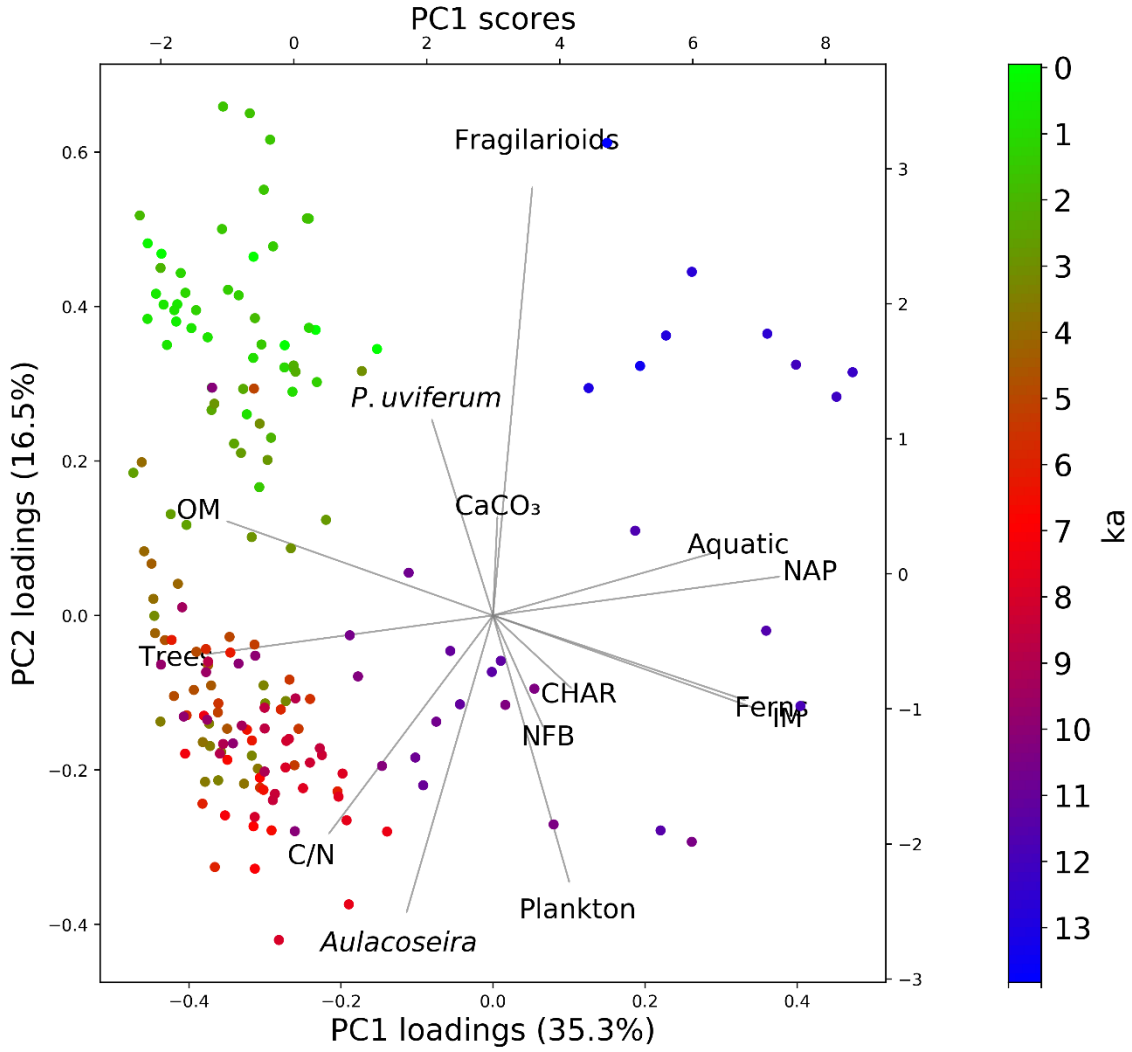

Figure 7. Biplot of principal component analysis applied to the most selected multiproxy data. The color of each observational level (dots) corresponds to the date shown by the color bar to the right.

Table II Loadings of Multiproxy PCA

Component	Variance explained	Positive	Negative
Multiproxy PC1	35.3%	NAP*:* **0.42** Inorganic matter: **0.39** Ferns: **0.37** Aquatics: **0.32** CHAR: **0.13** Plankton: **0.11** NFB: **0.07** Small fragilarioids: **0.06** $CaCO_3$: **0.01**	Trees*:* **-0.42** Organic matter: **-0.39** C/N: **-0.24** *Aulacoseira*: **-0.13** *Pilgerodendron uviferum*: **-0.09**
Multiproxy PC2	16.5%	Small fragilarioids: **0.61** *Pilgerodendron uviferum*: **0.28** $CaCO_3$: **0.14** Organic matter: **0.13** Aquatics: **0.09** NAP: **0.06**	*Aulacoseira*: **-0.42** Plankton: **-0.38** C/N: **-0.31** NFB: **-0.16** Inorganic matter: **-0.13** Ferns: **-0.12** CHAR: **-0.10** Trees: **-0.06**

The evolution of multiproxy PC1 (Figure 8.a) features strong positive deviations between ~13.8-11.4 ka, at which point values start to decrease until reaching a local minima at ~9.7 ka, albeit presenting a pronounced positive reversal between ~10.5-10.3 ka. Subsequently, the multiproxy PC1 values remain primarily negative until present, with slight positive punctuations at ~7.8-7.4 ka, ~6.1 ka, ~3 ka, and present. The multiproxy PC2 time series (Figure 8.b) commences with a strong positive deviation that immediately continues with a negative trend until reaching a global

minima between ~7.9-7.4 ka. Afterwards, the multiproxy PC1 time series shows a positive trend that culminates at ~1.6 ka with a global maxima, albeit a conspicuous negative reversal between ~3.8-3.1 ka.

Multiproxy k-means analysis

I used these same variables to generate a k-means analysis with 4 clusters (Figure 8 and 9). The first multiproxy cluster (MC1; cyan) is associated with high values of IM, small fragilarioids, NAP, ferns, and aquatics, and low values of $CaCO_3$, OM, C/N, CHAR, trees, and *Pilgerodendron uviferum*. MC1 was assigned to the oldest portion of the record, between ~13.8-11.5 ka (Figure 8.c). The second multiproxy cluster (MC2; red) is associated with high values of C/N, plankton, NFB, and CHAR, and low values of small fragilarioids and *P. uviferum*. MC2 was assigned to the following sections: ~11.3-10.7 ka, ~10.1-9.9 ka, ~9.4-7.4 ka, ~6.1-5.2 ka, ~4.2 ka, and ~3.8-3.5 ka. The third multiproxy cluster (MC3; white) is associated with high values of *Aulacoseira* and low values of small fragilarioids, plankton, NFB, CHAR, ferns, and aquatics. MC3 assignations alternate with MC2 and are most prominently found at ~10.4-10.2 ka, ~9.8-9.5 ka, ~7.3-6.2 ka, ~4.9-4.4 ka, ~4.1-3.8 ka, and ~3.5-3.1 ka. Lastly, the fourth multiproxy cluster (MC4; green) is associated with high values of OM, small fragilarioids, trees, *P. uviferum*, and aquatics, and low values of IM, C/N, *Aulacoseira,* plankton, CHAR, NAP, and ferns. MC4 dominates assignations between ~3 ka and present, along with brief assignations at ~10.6 ka, ~10.1 ka, and ~5 ka.

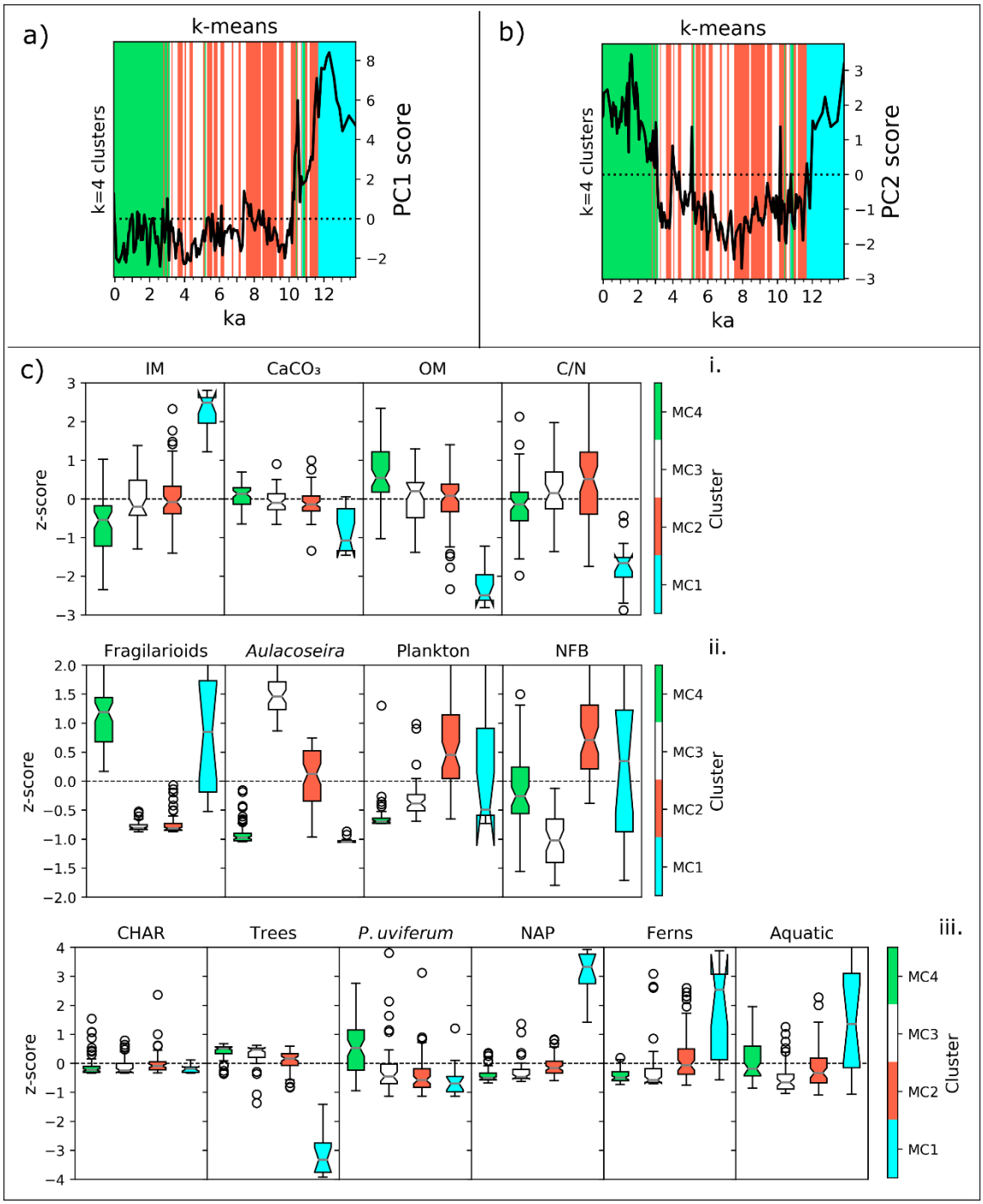

Figure 8. a) multiproxy PC1 time series over 4-cluster k-means analysis backdrop derived from the variables shown in c). b) same as a) but with multiproxy PC2 time series. c) box plots of each variable relating to each multiproxy cluster (MC).

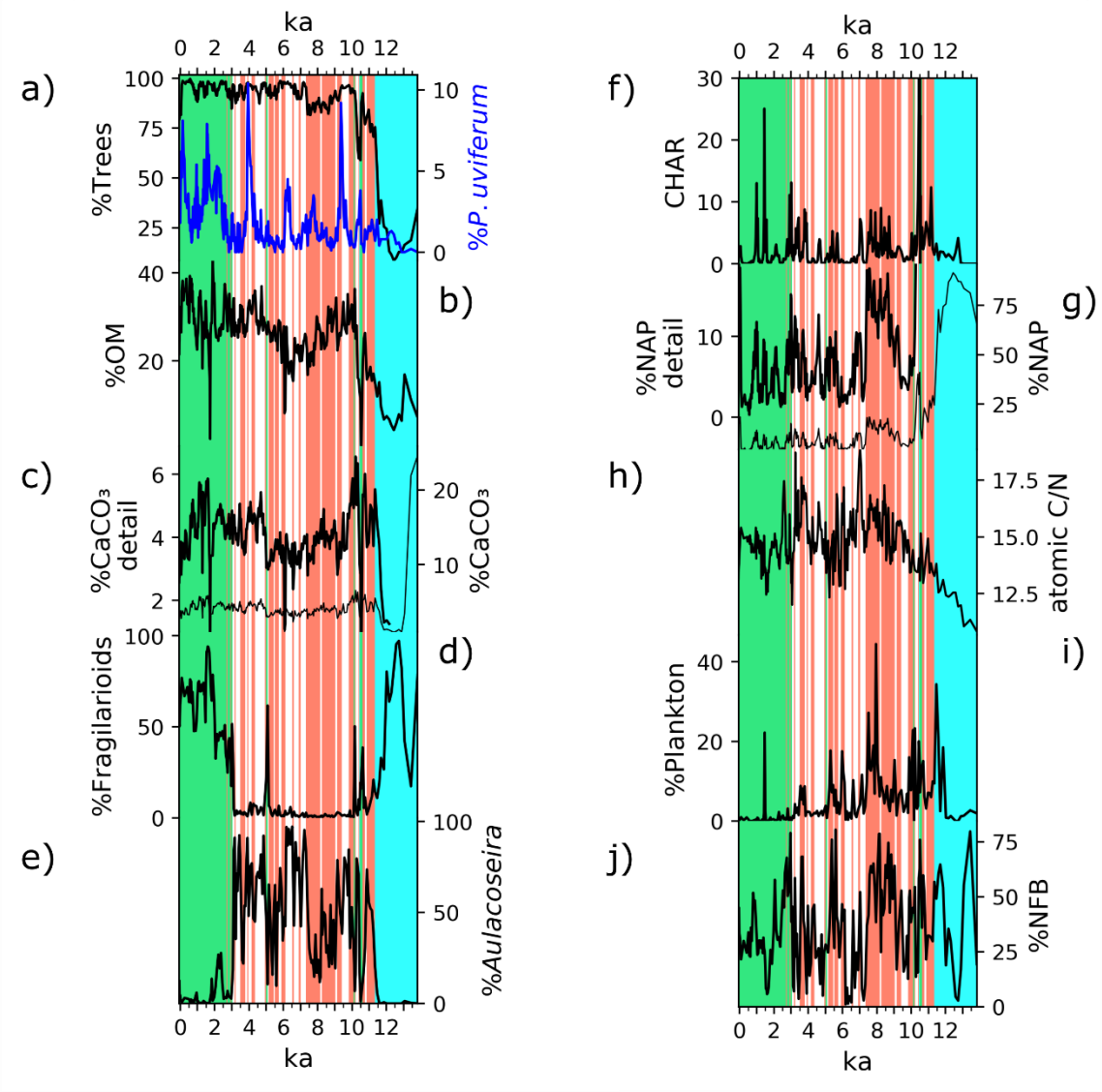

Figure 9. a). Time series of arboreal pollen (trees) abundance in black and *Pilgerodendron uviferum* abundance in blue. b) percent of organic matter (OM) from LOI data. c) percent of calcium carbonate from LOI data. d) time series of small fragilarioid abundance. e) time series of *Aulacoseira* abundance. f) macroscopic charcoal accumulation rates (CHAR) time series. g) abundance of non-arboreal pollen (NAP). h) atomic C/N time series. i) time series of plankton abundance. j) time series of non-small fragilarioid benthos (NFB) abundance. All time series overlay 4-cluster k-means analysis backdrop.

DISCUSSION

Diatom diversity

The LC diatom record features numerous taxa considered as endemic to the sub-Antarctic region (Table SI). A vast majority of the biodiversity is held by pennate forms, arguably benthics, chain-forming small fragilarioids, and species of the genus *Aulacoseira*. The latter, however, exhibits the largest abundance throughout the entire record. Few of the taxa found can be categorized as true planktonic diatoms. Due to the endemic nature of some of the most frequent taxa found, limnological inferences are relegated to a general functional grouping.

I will discuss the ecological implications of the most common diatom groups before discussing the inferred lake evolution. First, small fragilarioids prominently occupy CIP-1 and the zones CIP 9-10, but are virtually absent over the interval between CIP 2-8, with slight incursions in CIP-7. Notably, neither plankton nor *Aulacoseira* cooccur during small fragilarioid-rich periods, with the exception of CIP-2, when small fragilarioid abundance was being replaced by plankton and *Aulacoseira* abundance, and CIP-9, when *Aulacoseira* abundance was being replaced by small fragilarioid abundance. Lake surface ice may be an environmental factor that would favor small fragilarioids by warding off plankton and *Aulacoseira*, as the latter require ice-free conditions to occupy the water column. Lentic environments that are almost permanently frozen over have been commonly documented to be dominated by small fragilarioids (Fey et al., 2009; Fritz and Anderson, 2013; Lotter and Bigler, 2000; Smol and Douglas, 2007). As temperature increases throughout the annual cycle, ice first melts around the shallow lake periphery, where cold-tolerant small fragilarioid and benthic species may thrive (Lotter and Bigler, 2000). Lake level

lowering may be ruled out as the driving factor of small fragilarioid proliferation given that such conditions tend to also favor NFB species (Smol and Douglas, 2007), however, a broader range of NFB diversity and abundance appear during small fragilarioid-poor periods such as CIP-4, CIP-6, and CIP-8. Additionally, the small fragilarioid-rich intervals CIP 9-10 alternate with NFB species. This, in sum with the fact that a local small fragilarioid maxima at ~1.7-1.5 ka overlays a 3-cm thick tephra, when after small fragilarioids thrive and benthic/epiphytic species decline, supports the premise that small fragilarioids may support more ecologically harsh conditions (e.g., prolonged freeze-over or tephra induced light shielding), as they are common early colonizers (Fernández et al., 2013). I therefore interpret that high small fragilarioid abundance may be indicating prolonged lake-freezing seasons in LC.

Second, I note a synchronous proliferation of the NFB *Planothidium aueri* and *Achnanthidium spp. cf. minutissimum* and the planktonic *Discostella pseudostelligera* (abbreviated as *PAD* assemblage) in CIP-4, CIP-6, and CIP-8. In line with the possibility that the ice-cover regime may be the driving factor of diatom assemblages in LC, the co-occurrence of NFB and planktonic species is coherent with a reduced or absent lake freezing season through the annual cycle under warmer conditions. In this scenario, the plankton would benefit from an early ice-off date, pronounced stratification, and nutrient cycling (Wiltse et al., 2016), while the NFB would benefit from lake-level lowering, developed littoral environments, and enhanced transparency (Vermaire and Gregory-Eaves, 2007). Conversely, lake-level rise as an explanation more typically suited for planktonic development may be ruled out given that this would limit light penetration to NFB habitats, but rather I observe that these two groups systematically and concordantly fluctuate throughout the LC record. I therefore interpret that the abundance of the *PAD*

assemblage in the LC record may indicate ice-free conditions with sufficient stratification and transparency for synchronous planktonic and NFB development.

Third, at the interval CIP 2-8, the most ubiquitous diatom in the LC record, *Aulacoseira humilis/liucoensis*, experiences high amplitude fluctuations that are generally antiphased with other functional groups (Figure 4). The abundance of this taxon repeatedly oscillates from values as low as 10% to over 75% on millennial time scales. Millennial-scale high-stands for this taxon occur during CIP-3, CIP-5, and CIP-7, alternating with low-stands during CIP-4 and CIP-6. Sub-millennial scale fluctuations are antiphased with the *PAD* assemblage previously discussed. *Aulacoseira* are heavily silicified diatoms which require turbulence to stay afloat in the water column (Rühland et al., 2015). Further ecological inference is occluded by the limited information available for the species involved. Notwithstanding, several published studies related with *Aulacoseira* paleoecology (Denisov and Genkal, 2018; Enache and Prarie, 2000; Fey et al., 2009; García et al., 2019; Genkal and Kulikovskiy, 2014; Laing and Smol, 2003; Mayr et al., 2019; Neil et al., 2019; Siver and King, 1997; Stevenson et al., 1991; Trifonova and Genkal, 2000) suggest that, under the conditions applicable to LC, *Aulacoseira humilis/liucoensis* may indicate turbulence – via physical or thermal mixing – as well as considerably long ice-free seasons with sparse macrophyte cover (See *Supplementary Material* Discussion on the autoecology of *Aulacoseira humilis/liucoensis*). Ice-free and turbulent lake conditions are therefore the most likely prerequisites for *Aulacoseira* proliferation, from which I interpret that *Aulacoseira* presence in the LC record may indicate an intermediate condition between small fragilarioid-rich and *PAD*-rich periods, summarized as temperate and windy.

Lake evolution inferred from fossil diatom assemblages

The diatom PC1 curve (Figure 6 and 7) captures: (i) the *PAD* assemblage at the most positive end, interpreted as ice-free conditions; (ii) *Aulacoseira humilis/liucoensis* with positive to near-mean values, indicative of temperate and windy LC conditions; and (iii) small fragilarioid-dominated assemblages at the negative end, interpreted here as akin to prolonged freeze-over conditions. The most positive deviations occur between ~9-7.4 ka, followed by ~5.6-5.3 ka and ~3.8-3.1 ka intervals. Pronounced negative diatom PC1 deviations occur during the ~14.2-11.7 ka and ~3-0 ka intervals. I posit that diatom PC1 captures the most salient and contrasting hydroclimatic fluctuations. On the other hand, the diatom PC2 separates NFB from *Aulacoseira humilis/liucoensis* and thus may track the degree of littoral development with positive values, as opposed to predominant water-column occupation with negative values.

To track the statistically significant recurrence of diatom assemblages throughout the record I developed a k-means analysis using the time series of the two most prominent diatom groups, small fragilarioids and *Aulacoseira* (Figure 6). Based on the clustering results derived from these factors (Figure 6), I interpret DC1 as a hallmark of small fragilarioid dominance, related to cold/wet conditions, DC2 as akin to *PAD,* related to warm/dry conditions, DC3 as akin to *Aulacoseira,* indicative of the temperate and turbulent conditions.

With the combined multivariable methods applied to the diatom data, I interpret the following lake evolution of LC (Figure 8). The oldest portion of the record, between ~14.2-11.6 ka shows negative diatom PC1 values and DC1 assignations, which suggest prolonged ice-cover through the annual cycle under cold/wet conditions. Low DAR during this interval suggest low productivity that veer gradually towards warmer/drier conditions by ~12 ka. The subsequent appearance of planktonic diatoms suggests longer ice-free periods during the annual cycle and higher stratification. An abrupt increase in *Aulacoseira* at ~11.2 ka marks the onset of highly

variable lake conditions that persist until ~9 ka, shifting through all DC assignations with near-mean to positive diatom PC1 values. This heterogeneity indicates reversible fluctuations between cold, temperate, and warm conditions, along with variable lake mixing regimes. The diatom PC1 curve shows conspicuous step-wise increments between ~9-7.4 ka, along with a concentrated block of DC2 assignations that I interpret as a stable period of warm/dry stratified conditions with an early-ice off date through the annual cycle.

An abrupt shift toward positive to near-mean diatom PC1 values and a predominance of DC3 assignations marks a transition to temperate and turbulent conditions between ~7.4-3.1 ka. During this multi-millennial *Aulacoseira*-dominant interval, I observe short-lived intervals of higher stratification and/or earlier ice-off date occur between ~5.6-5.3 ka and ~3.8-3.1 ka, indicative of warm/dry spells. The latter of these brief intervals shows higher variability along with reduced productivity since ~5 ka.

An abrupt transition to negative diatom PC1 values and prominent DC1 assignations ensued, which I interpret as extended freeze-over seasons under cold/wet conditions from ~3.1 ka to the present. Increased DAR values since ~2.8 ka accompanied by abrupt compositional changes within the small fragilarioid group suggest increased productivity during this interval.

Environmental evolution of LC

I developed a multiproxy PCA with the data published in Moreno et al. (2018c), that includes LOI and elemental analysis, CHAR, and fossil pollen. The multiproxy PC1 chiefly represents important changes among terrestrial proxies, such as NAP and LOI data, whereas the multiproxy PC2 represents important changes occurring in diatom assemblages, as well as C/N, CHAR, and *Pilgerodendron uviferum* data. By this merit, the multiproxy PC1 is similar to the NAP data that

has already been analyzed in Moreno et al. (2018c) where Cipreses cycles (CCs) were derived from positive deviations in this series during Holocene. Therefore, more attention will be given to the multiproxy PC2, that may offer a new dimension of hydroclimatic resolution that has not yet been analyzed.

The structure of multiproxy PC2 series is similar -although inverse- to that of the diatom PC1 series, which is unsurprising given that small fragilarioids and *Aulacoseira/*plankton show the highest positive and negative loadings, respectively. The differences reside in the information given by the C/N, CHAR, $CaCO_3$, and *Pilgerodendron uviferum* values, where $CaCO_3$, and *P. uviferum* correlate with small fragilarioid abundance, C/N with *Aulacoseira* abundance, and CHAR with NFB and plankton abundance. These associations may indicate a coupling between climate-mediated terrestrial input and diatom assemblages.

For example, higher C/N values could portray increased terrestrial input related with runoff which is coherent with the temperate, windy, and ice-free conditions inferred by high *Aulacoseira* abundance. Furthermore, although warm/dry periods would also favor higher C/N values through littoral development, these fire-conducive conditions have a stronger association with increased CHAR and NAP values, which is coherent with coeval increments of plankton and NFB. On the other hand, low values of C/N may indicate higher algal input which is coherent with higher small fragilarioid abundance during periods of prolonged freeze-over seasons through the annual cycle. Concomitantly, the inferred prolonged freeze-over seasons in the youngest portion of the record would influence $CaCO_3$ precipitation rates given that CO_2 would remain trapped within the water column under these conditions (Fritz and Anderson, 2013). The coeval increase of hygrophilous and cold-tolerant *P. uviferum* is also compatible with these inferences. It may

therefore be argued that positive (negative) multiproxy PC2 values are indicative of cold/wet (warm/dry) conditions.

To consolidate these findings, I developed a multiproxy k-means analysis to the track the statistical recurrence of changes in these terrestrial and aquatic environmental sensors (Figure 8 and 9). This analysis led to the distinction of four clusters:

- MC1, that presents an affinity to simultaneous high inorganic matter, NAP and small fragilarioid abundance, which I interpret as the absence of forest and presence of alpine herbs and grasses (i.e., *Gunnera*) during cold/hyperhumid conditions that favored cold-tolerant small fragilarioids under nutrient-limited and prolonged freeze-over season through the annual cycle;
- MC2, that is centered around increments of C/N, CHAR, NAP and plankton/NFB abundance, which I interpret as periods of fire-induced canopy aperture under warm/dry conditions that also result in higher lake stratification, littoral development, and/or earlier ice-off date through the annual cycle.
- MC3, that is most akin to high *Aulacoseira* abundance, which I interpret as indicating temperate and windy conditions that present sufficient wind-driven lake turbulence and ice-free conditions to favor the development of heavily silicified *Aulacoseira*; and
- MC4, that is influenced by high values of organic matter, $CaCO_3$, trees, *P. uviferum* and small fragilarioid abundance and, conversely, low NAP and plankton abundance, which I interpret as indicating closed-canopy surroundings under cold/wet conditions with prolonged freeze-over season through the annual cycle;

This ordination suggests the following phases in the environmental reconstruction of LC and its watershed (Figure 9). MC1 between ~14.2-11.4 ka identifies a colder and wetter than-present interval, which uniquely features low fire activity coeval with peak NAP and small fragilarioid abundance. An attenuation of these indicators near ~12 ka suggests a warming trend. Subsequently, MC2, MC3, and MC4 alternate between ~11.4-9 ka as fire activity in conjunction with planktonic/NFB and *Aulacoseira* abundance undergo centennial-scale alternations. Unstable centennial-scale climate patterns could account for the alternating clusters under temperate to warm/dry conditions. This high variability terminates with a continuous MC2 assignation between ~9-7.4 ka. I interpret this interval as the most stable period with extended ice-free conditions and most developed lake stratification under warm/dry conditions, coeval with enhanced fire activity, canopy aperture, and high C/N values. MC2 and MC3 assignations show centennial-scale alternations between ~7.4-3.1 ka, diagnostic of fluctuations between temperate/windy to warm/dry conditions. Extended temperate/windy (warm/dry) conditions occurred between ~7.3-6.2 ka and ~5.1-3.4 ka (~6.1-5.2 ka and ~4.3-3.5 ka) when fire activity was generally muted (enhanced). Lastly, I interpret the virtual permanence of MC4 assignation from ~3.1 ka to the present as indicative of a drastic environmental shift towards cold/wet conditions that favored the expansion of cold-tolerant hygrophilous conifer *Pilgerodendron uviferum* and small fragilarioids that could resist prolonged freeze-over seasons through the annual cycle. This period also features contemporary increases in diatom productivity related to small fragilarioid abundance.

Regarding the frequency of environmental or climate variability, I note three distinct large-magnitude multi-millennial-scale changes (~14.2–11.4 ka, ~11.4–3.1 ka, and ~3.1–0 ka) overprinting iterative sub-millennial fluctuations of lower magnitude. I applied a regime shift

detection (RSD) algorithm to the diatom PC1 and multiproxy PC2 time series to detect significant changes in mean and variance throughout the record (Figure 10; Rodionov, 2004). Significant changes in mean are in close accordance with the multimillennial blocks described above. For both series, the RSD algorithm indicates that a significant increase in variance occurs at ~4 ka. This could mark the onset of higher frequency environmental and/or climate variability in LC, which is compatible with the coeval train of CCs derived from the NAP time series.

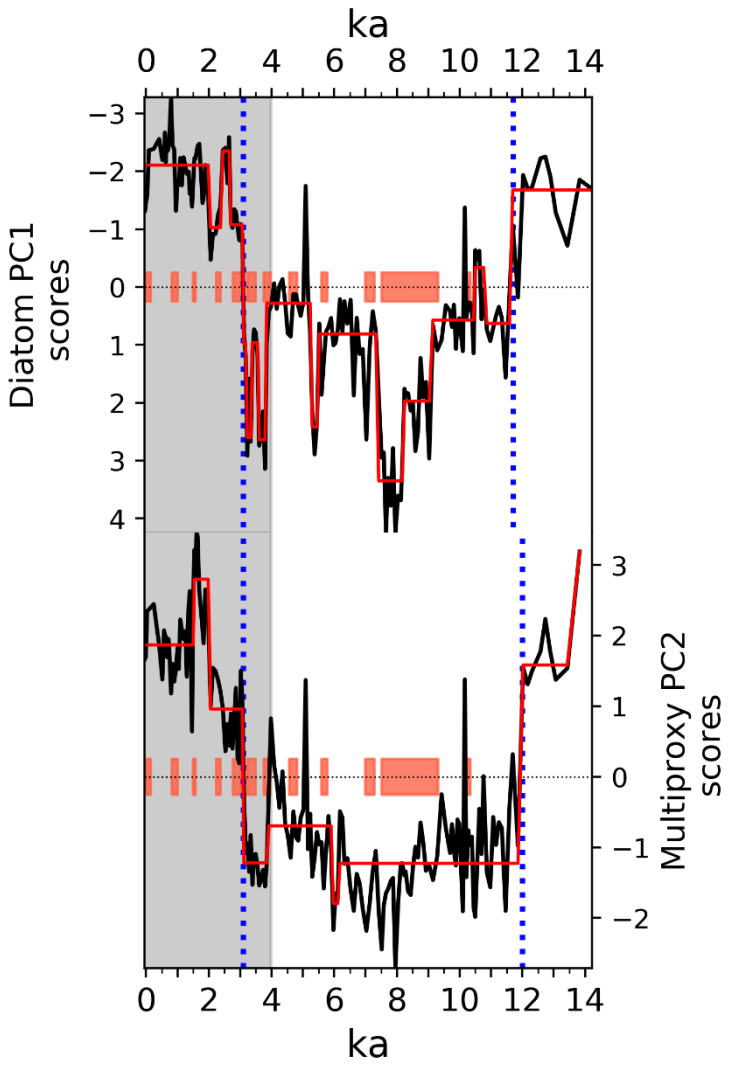

Figure 10. Time series of diatom PC1 (inverted y-axis) and multiproxy PC2 in black. Regime shift detection (RSD) algorithm applied to the mean in red (0.1 significance). Dotted blue lines mark timing of important multimillennial shifts. Grey ribbon represents section when RSD algorithm detects a significant increase in variance (0.05 significance). Light red boxes mark Cipreses Cycles from Moreno et al. (2018c).

Regional Implications

Late Glacial

I interpret a gradual transition between ~14.2-12 ka from intense cold/wet to temperate conditions, and then to warm/dry conditions by ~11.4 ka in LC. This is compatible with the rise in regional treeline under humid conditions implied by the steady increase in arboreal pollen in replacement of cold-adapted heathland during this time (Moreno et al., 2018c, 2021). This signal marks a shift from pioneer, early successional heath- and scrublands following glacial and glaciolacustrine recession/regression in the LC sector that took place during the earliest stages of T1 (Moreno et al., 2012, 2021). Warming temperatures are a likely explanation for the transition from small fragilarioid to planktonic importance. During this warming interval, however, significant amounts of small fragilarioids still remain, which could indicate colder-than-present temperatures and/or considerable surface-ice seasonality (Figure 9). Based on these considerations, I infer peak SWW influence at ~12.6 ka over SWP that steadily debilitated with step-wise inflection points at ~12 ka and ~11.4 ka.

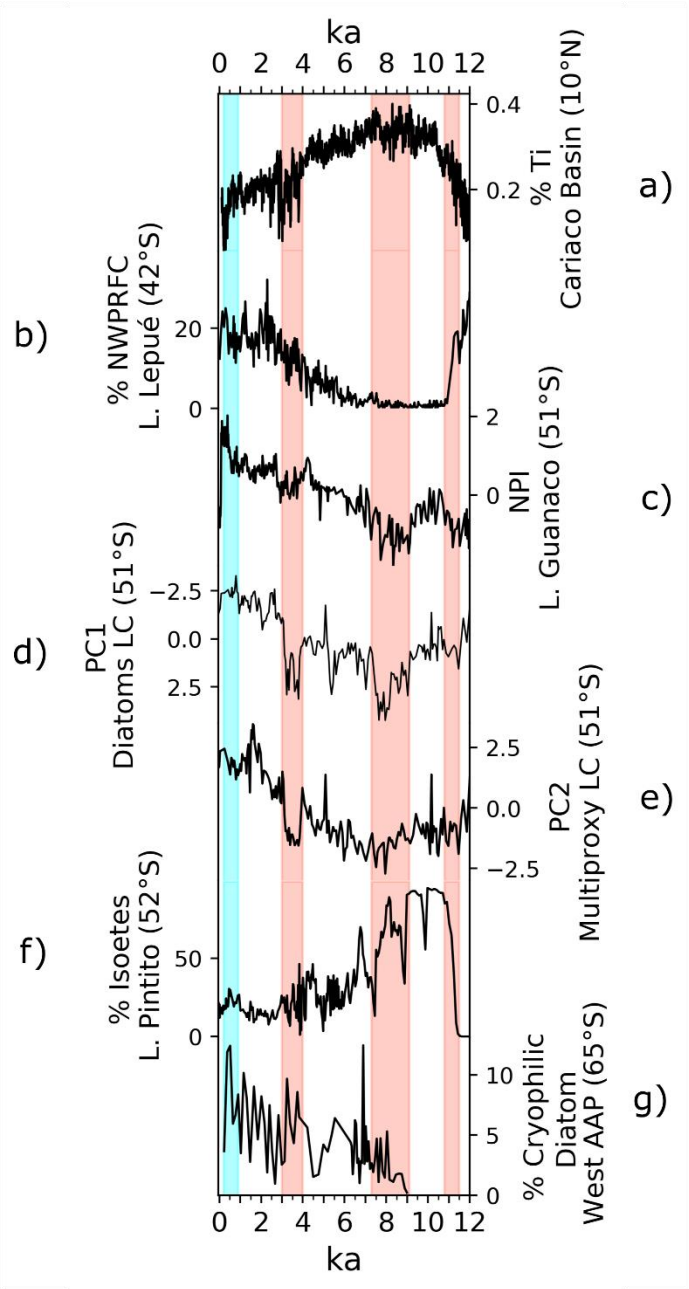

Figure 11. a) Time series of %Ti from Cariaco Basin (10°N; Haug et al., 2001) associated with latitudinal shifts of the ITZC. b) abundance of Northwestern Patagonian Rainforest Conifers (NWPRFC) from Lago Lepué (42°S; Pesce and Moreno, 2014). c) *Nothofagus*/Poaceae index (NPI) from Lago Guanaco (51°S; Moreno et al., 2010). d) diatom PC1 time series from this study (inverted y-axis). e) multiproxy PC2 time series from this study. f) abundance of *Isoëtes* from Lago Pintito (52°S; Moreno et al., 2021). g) abundance of cryophilic diatom, *Thalassiosira antarctica* 1, from core JPC-10 in western Antarctic Peninsula (AAP) (65°S; Etourneau et al., 2013). Pink (cyan) ribbons represent inferred weak (strong) SWW inferred from LC.

Early Holocene

Highly variable conditions persist in LC between ~11.4-9 ka, superseded by stable warm/dry conditions until ~7.4 ka. The latter period replicates pronounced negative *Nothofagus/*Poaceae index (NPI) values from Lago Guanaco (~30 km north of LC) related to negative hydrological balance (Moreno et al., 2010). Also, the littoral macrophyte *Isoëtes* rose at ~11.4 ka and reached a maximum until ~9.1 ka in the Lago Pintito record (~80 km south of LC), replicating the timing and direction of change towards warmer/drier conditions seen in LC (Figure 11.f). Moreover, terrestrialization, enhanced fire activity, and parkland expansion is common among palynological sites from Lago Argentino (50°S), TDPNP (51°S), and Seno de Última Esperanza (52°S) during this interval, all of which point toward negative hydrologic balance at regional scale (Moreno et al., 2012, 2018b, 2021; Wille and Schäbitz, 2009). Although controversial, the pollen record from Lake Tamar (~53°S), located along the Tamar fjord west of Gran Campo Nevado, shows an increase in hemiparasite *Misodendrum* pollen between ~11-9.1 ka and a sustained minimum of moorland vegetation between ~9.3-8 ka (Lamy et al., 2010), both of which could be understood as indicating warmer/drier conditions in the hyperhumid maritime sectors west of the Andes. Lamy et al. (2010), however, interpreted *Misodendrum* abundance as enhanced moisture despite the declining presence of hygrophilous moorland vegetation. Nevertheless, based on the LC results, I interpret weak and variable SWW influence over SWP between ~11.4-9 ka, followed by minimal SWW influence between ~9-7.4 ka. Strong SWW influence over LC would be counter to the inferred periods of ice-free conditions, prerequisite for planktonic and *Aulacoseira* development.

Mid Holocene

Warm/dry conditions vanish abruptly after ~7.4 ka when wind-derived water column mixing and moderate surface freezing duration, most likely under stronger SWW influence, ensued between ~7.4-6.1 ka and ~5.1-3.8 ka. In the interim, warm/dry conditions bracketed between ~6.1-5.2 ka punctuate the otherwise temperate climate conditions in LC (Figure 11.d). This warm/dry period is not recorded in the Lago Guanaco NPI record nor the Lago Pintito Isoëtes record, suggesting that the LC diatom record may be more sensitive to small magnitude climatic changes that do not surpass necessary physiological thresholds for a terrestrial ecosystem imprint. Weaker SWW influence over SWP could account this period.

Late Holocene

Warm/dry anomalies have been grouped under a Late Holocene Warm Period (LHWDP; Moreno et al., 2018) between ~4-2.7 ka, consistent with periodic early ice-off stratified conditions seen by the diatom record. Woodland opening in Lago Guanaco between ~4.1-2.9 ka (Moreno et al., 2009a) and sparse fire activity in TDPNP and Grand Campo-2 (~140 km south of LC) (Fesq-Martin et al., 2004; Moreno et al., 2018b) overlap well with this interval. I interpret these climatic cues as signs of variable weakening of SWW influence over SWP during this interval.

As discussed, the most recent portion of the Holocene (~3.1–0 ka) represents the coldest/wettest conditions in LC since the late glacial. This interpretation is compatible with highest NPI values from Lago Guanaco (Moreno et al., 2010), as well as the maximum spread of nearby Magellanic forest from other records which suggest a positive hydrological balance (Huber and Markgraf, 2003; Moreno et al., 2009a; Villa-Martinez and Moreno, 2007). I interpret strengthening of SWW influence over SWP during this period.

Global climate implications

At multi-millennial scales I infer anomalously low SWW influence over SWP bracketed between ~11.4-7.4 ka, followed by moderate influence until ~3.1 ka, at which point I appraise the strongest SWW influence thereafter. The latter is comparable in magnitude to the conditions observed between ~14.2-11.4 ka. At centennial timescale I detect high SWW instability between ~11.4-9 ka, followed by a stable SWW nadir until ~7.4 ka, after which reversible centennial-scale fluctuations occur with intervals of SWW wanning clustered at ~6.1-5.2 ka and ~3.8-3.1 ka. Additionally, higher hydroclimatic variance is prominently established at ~4 ka. In the following paragraphs I will compare these inferences of SWW change with paleoclimate records from other regions to assess potential drivers.

Stronger-than-present SWW between ~14.2-11.4 ka was contemporary with a southward migration of the ITCZ in the South American continent that reaches its southernmost position by the end of this period (Haug et al., 2001). The following inception of a northward ITCZ trend is roughly synchronous with stark subcontinental-scale evidence of weakened SWW between ~11.4-7.4 ka (Figure 11.a). I base this claim on evidence from the SWW core-region (longer ice-free growing seasons in LC, lake level drop in Lago Pintito [Moreno et al., 2021]), lake-level drop in Lago Lepué ~950 km north of LC (Pesce and Moreno, 2014), and reduced mire surface wetness in Punta Burslem ~500 km southeast of LC (McCulloch et al., 2020). Concomitant warming and reduced sea ice in the Antarctic Peninsula (AAP; Figure 11.g) has been interpreted in terms of a strong, poleward contracted SWW belt (Etourneau et al., 2013; Mulvaney et al., 2012; Shevenell et al., 2011). As noted in Moreno et al. (2021) stronger SWW at the latitudes of the Drake Passage during this time would most likely exert higher surface wind stress over the Southern Ocean which, in turn, should lead to enhanced deep-water ventilation of old CO_2. However, the

converse has been evidenced (stagnate or declining atmospheric CO_2 concentrations that reach isotopic equilibrium), which lends more credibility to an overall debilitated SWW belt (Monnin et al., 2001; Schmitt et al., 2012). Moreover, SWW circulation may have weakened under reduced meridional atmospheric pressure gradients associated with a north shifting ITCZ and anomalously warm high latitudes (Haug et al., 2001; Mulvaney et al., 2012).

I note that a tipping point in SWW behavior at ~9 ka. Before ~9 ka, the LC record suggests higher SWW '*flickering switch'* variability, also detected in other southern Patagonian sites (McCulloch et al., 2020; Wille and Schäbitz, 2009). This suggests progressive SWW weakening as the ITCZ reached its northernmost position (Haug et al., 2001). Also, an ice-core from the eastern AAP show that surface-level atmospheric temperature decreased from a maximum at ~11.8 ka to mean values at ~9.2 ka (Mulvaney et al., 2012). Taken together, the tropical and extra-tropical climatic trends before ~9 ka may have played role in SWW variability, whose subsequent stabilization is reflected by a period of sustained SWW attenuation.

Enhanced SWW influence in SWP by ~7.4 ka was synchronous (within dating uncertainties) with Northwestern Patagonian (NWP) sites. At this point transgressive lake phases develop in Lago Lepué (~43°S), Lago El Salto (~41°S), and Lago Pichilaguna (~41°S) based on shifting abundances of *Isoëtes* (Moreno and Videla, 2016; Moreno et al., 2018a; Pesce and Moreno, 2014). By ~6.7 ka, a positive trend of NWP Rainforest conifers (NWPRFC) in Lago Lepué also commences (Pesce and Moreno, 2014; Figure 11.b) which may also be associated with positive hydrological balance. An equatorward SWW intensification could explain enhanced SWW influence in SWP and NWP, as well as transgressive lake phases in central Chile by ~6 ka (Frugone-Álvarez et al., 2020; Jenny et al., 2003; Valero-Garcés et al., 2005). South tracking ITCZ (Haug et al., 2001) and expanded sea

ice in the AAP (Etourneau et al., 2013) may have configured increasing meridional atmospheric pressure gradients compatible with stronger SWW.

Periodically weakening SWW influence in SWP between ~4-2.7 ka corresponds to the LHWDP which have been attributed to positive SAM-like poleward SWW contractions at centennial timescale (Kaplan 2020; McCulloch et al., 2020; Moreno et al., 2018c; Reynhout et al., 2019). Conspicuous large-magnitude latitudinal ITCZ fluctuations coeval with this period may express the working of a common forcing resulting in equally important SWW shifts clustered in this interval. These SWW shifts are, however, superimposed upon trends of SWW strengthening in SWP (see Lago Pintito *Isoëtes* minimum Figure 11.f; Moreno et al., 2021; Moy et al., 2011). Additionally, studies from the AAP, apart from suggesting warming and glacial retreat (Kaplan et al., 2020; Mulvaney et al., 2012; Shevenell et al., 2011), show increasing abundance of biochemical markers and diatom assemblages associated with increasing sea ice presence as well as open ocean conditions (Etourneau et al., 2013), possibly pointing towards increased seasonality at higher latitudes. The results from LC suggest that covariability between low and high latitudes involved changes in SWW strength or latitudinal position (Pesce and Moreno, 2014).

Strong SWW influence over SWP between ~2.7-0 ka was synchronous with southward-shifted ITCZ (Haug et al., 2001), the highest Holocene abundance of NWPRFC in Lago Lepué (Pesce and Moreno, 2014), and a renewed trend of surface-level atmospheric cooling and peak abundance of cryophilic diatoms in the AAP (Mulvaney et al., 2012; Etourneau et al., 2013; Figure 11.g). Further SWW strengthening in SWP may have developed through this tropical and extra-tropical configuration under steepened meridional atmospheric pressure gradients. The fact that the

conditions that developed in LC at ~2.7 ka are similar to the ones recorded presently, may indicate that the current SWW positioning and behavior emerged at this point.

Instrumental records have captured interannual and interdecadal variability in current climate. The synoptic scale weather patterns that determine the climate of SWP are principally influenced by interannual SAM variability. This makes LC a satisfactory sensor of centennial-scale SAM-like changes throughout the past. I note, however, that a simple association between weak (strong) SWW over SWP and positive (negative) SAM-like conditions may not be confidently applicable throughout the entire Holocene. For example, positive SAM-like conditions between ~6.1-5.2 ka cannot explain the strengthened SWW further north. The significantly different tropical-extratropical configuration at this time may have triggered significantly different SWW responses (i.e., equatorward SWW expression), thus posing the possibility of non-stationary tropical and extra-tropical teleconnections. In other words, during this interval (~6.1-5.2 ka), the alleged northward ITCZ position may have affected how ENSO and SAM interact, bringing about SWW behavior that is outside of the range of possibilities under the current climate conditions. SAM and ENSO reconstructions that span the last millennium have emphasized that spatial correlations with these climate modes are non-stationary (Dätwyler et al., 2018), and furthermore, that an expected negative correlation between SAM and ENSO phases is rarely significant (Dätwyler et al., 2020). Gomez et al. (2011) suggests similar non-stationary interplay between ENSO and SAM on millennial time scales, such that in-phase or out-of-phase oscillations may produce amplifying or neutralizing effects. Because of this, I suggest that the LC reconstruction here presented affords more confident centennial-scale SAM-like interpretations since ~2.7 ka.

Indeed, exacerbated ENSO development coincides with the onset of higher inferred hydroclimatic variance since ~4 ka (Conroy et al., 2008; Moy et al., 2002). This may be a telltale sign that tropical and extra-tropical climate covariability has evolved throughout the Holocene, and that the SWW play a fundamental role in propagating climate changes associated with internal variability (Moreno, 2002; Moreno et al., 2018c; Dätwyler et al., 2020; Fogt and Marshall, 2020).

CONCLUSIONS

The coupled diatom, pollen, and CHAR environmental reconstruction of LC reveals the following:

(I)

(i) Stronger SWW influence over SWP between ~14.2-12 ka seen by a high abundance of cryophilic small fragilarioids that may indicate extended freeze-over seasons through the annual cycle. This occurs in the context of cold-tolerant hygrophilous vegetation and muted fire activity.

(ii) A step-wise SWW weakening at ~12 ka and ~11.4 ka seen by the appearance of plankton and then *Aulacoseira*, concomitant with plummeting small fragilarioids, that may indicate shortening freeze-over seasons through the annual cycle. This occurs in the context of forest expansion and incremental fire activity. The SWW belt could either have shifted poleward or started to generally debilitate.

(iii) Variable and weakening SWW behavior between ~11.4-9 ka, seen by shifting mixed clusters that represent fluctuating lake freezing and mixing regimes. This occurs in the context of closed-canopy development and enhanced fire activity. The SWW belt is inferred to have become weaker and more erratic.

(iv) A stable period of weak SWW influence between ~9-7.4 ka seen by high abundance of plankton and NFB species that may reflect periods of higher lake stratification and earlier ice-off date through the annual cycle. This occurs in the context of forest canopy

aperture and sustained fire activity. The SWW belt is inferred to have stabilized in a weak condition.

(v) An abrupt transition to more SWW influence at ~7.4 ka that permits the development of *Aulacoseira* under ice-free turbulent lake conditions. This occurs in the context of closed-canopy forests with muted fire activity. The SWW belt is inferred to have revitalized.

(vi) The interruption of the temperate/windy conditions through SWW weakening over SWP between ~6.1 -5.2 ka and ~3.8 – 3.1 ka, seen by higher plankton and NFB abundance that signals shortened freeze-over seasons through the annual cycle. This occurs in the context of the forest canopy aperture and enhanced fire activity. The SWW belt is inferred to have diminished its influence over SWP during these periods.

(vii) SWW strengthening after ~3.1 ka, seen by a resurgence of small fragilarioids that may indicate extended periods of freeze-over seasons through the annual cycle. This occurs in the context of cold-tolerant conifer expansion. The SWW belt is inferred to have arrived at the current position by ~2.7 ka.

(II) Multivariable analysis permitted the detection of recurring environmental conditions and increased hydroclimatic variability since ~4 ka.

(III) Centennial-scale SAM-like interpretations are suggested to be less robust before ~2.7 ka due to an evolving covariability between tropical and extra-tropical climates.

REFERENCES

Abdi, H., & Williams, L. J. (2010). Principal component analysis. *Wiley interdisciplinary reviews: computational statistics*, *2*(4), 433-459.

Agosta, E., Compagnucci, R., & Ariztegui, D. (2015). Precipitation linked to Atlantic moisture transport: clues to interpret Patagonian palaeoclimate. *Climate Research*, *62*(3), 219-240.

Anderson, R. F., Ali, S., Bradtmiller, L. I., Nielsen, S. H. H., Fleisher, M. Q., Anderson, B. E., & Burckle, L. H. (2009). Wind-driven upwelling in the Southern Ocean and the deglacial rise in atmospheric CO2. *science*, *323*(5920), 1443-1448.

Aravena, J. C., & Luckman, B. H. (2009). Spatio-temporal rainfall patterns in southern South America. *International Journal of Climatology: A Journal of the Royal Meteorological Society*, *29*(14), 2106-2120.

Battarbee, R. W. (1986). Diatom analysis. *Handbook of Holocene palaeoecology and palaeohydrology*, 527-570

Blaauw, M., & Christen, J. A. (2013). Bacon Manual v2. 3.3.

Boisier, J. P., Alvarez-Garretón, C., Cepeda, J., Osses, A., Vásquez, N., & Rondanelli, R. (2018, April). CR2MET: A high-resolution precipitation and temperature dataset for hydroclimatic research in Chile. In *EGU General Assembly Conference Abstracts* (p. 19739).

Breuer, S., Kilian, R., Schörner, D., Weinrebe, W., Behrmann, J., & Baeza, O. (2013). Glacial and tectonic control on fjord morphology and sediment deposition in the Magellan region (53 S), Chile. *Marine Geology*, *346*, 31-46.

Chen, C., Zhao, W., & Zhang, X. (2021). Pacific Decadal Oscillation-like variability at a millennial timescale during the Holocene. *Global and Planetary Change*, *199*, 103448.

Conroy, J. L., Overpeck, J. T., Cole, J. E., Shanahan, T. M., & Steinitz-Kannan, M. (2008). Holocene changes in eastern tropical Pacific climate inferred from a Galápagos lake sediment record. *Quaternary Science Reviews*, *27*(11-12), 1166-1180.

Dätwyler, C., Neukom, R., Abram, N. J., Gallant, A. J., Grosjean, M., Jacques-Coper, M., ... & Villalba, R. (2018). Teleconnection stationarity, variability and trends of the Southern Annular Mode (SAM) during the last millennium. *Climate dynamics*, *51*(5), 2321-2339.

Dätwyler, C., Grosjean, M., Steiger, N. J., & Neukom, R. (2020). Teleconnections and relationship between the El Niño–Southern Oscillation (ENSO) and the Southern Annular Mode (SAM) in reconstructions and models over the past millennium. *Climate of the Past*, *16*(2), 743-756.

Denisov, D. B., & Genkal, S. I. (2018). Centric diatom algae of Lake Imandra (Kola Peninsula, Russia). *International Journal on Algae*, *20*(1).

Díaz Pardo, C. A., Echazú, D. M., & Maidana, N. I. (2008). Diatomeas continentales como indicadoras de cambios climáticos en Patagonia. *Efecto de los cambios globales sobre la biodiversidad*, 233-246.

Ding, Q., Steig, E. J., Battisti, D. S., & Wallace, J. M. (2012). Influence of the tropics on the southern annular mode. *Journal of Climate*, *25*(18), 6330-6348.

Enache, M., & Prairie, Y. T. (2000). Paleolimnological reconstruction of forest fire induced changes in lake biogeochemistry (Lac Francis, Abitibi, Quebec, Canada). *Canadian Journal of Fisheries and Aquatic Sciences*, *57*(S2), 146-154.

Etourneau, J., Collins, L. G., Willmott, V., Kim, J. H., Barbara, L., Leventer, A., ... & Massé, G. (2013). Holocene climate variations in the western Antarctic Peninsula: evidence for sea ice extent predominantly controlled by changes in insolation and ENSO variability. *Climate of the Past*, *9*(4), 1431-1446.

Fercovic, E. I., (2019). Evolución de la vegetación, regímenes de fuego y clima en el extremo suroriental de la Isla Grande de Chiloé desde el término de la Última Glaciación, Ms Thesis. Universidad de Chile, Santiago, 91 pp.

Fernández, M., Björck, S., Wohlfarth, B., Maidana, N. I., Unkel, I., & Van der Putten, N. (2013). Diatom assemblage changes in lacustrine sediments from Isla de los Estados, southernmost South America, in response to shifts in the southwesterly wind belt during the last deglaciation. *Journal of paleolimnology*, *50*(4), 433-446.

Fesq-Martin, M., Friedmann, A., Peters, M., Behrmann, J., & Kilian, R. (2004). Late-glacial and Holocene vegetation history of the Magellanic rain forest in southwestern Patagonia, Chile. *Vegetation History and Archaeobotany*, *13*(4), 249-255.

Fey, M., Korr, C., Maidana, N. I., Carrevedo, M. L., Corbella, H., Dietrich, S., ... & Zolitschka, B. (2009). Palaeoenvironmental changes during the last 1600 years inferred from the sediment record of a cirque lake in southern Patagonia (Laguna Las Vizcachas, Argentina). *Palaeogeography, Palaeoclimatology, Palaeoecology*, *281*(3-4), 363-375.

Filzmoser, P., & Todorov, V. (2013). Robust tools for the imperfect world. *Information Sciences*, *245*, 4-20.

Fogt, R. L., & Marshall, G. J. (2020). The Southern Annular Mode: variability, trends, and climate impacts across the Southern Hemisphere. *Wiley Interdisciplinary Reviews: Climate Change*, *11*(4), e652.

Fritz, S. C., & Anderson, N. J. (2013). The relative influences of climate and catchment processes on Holocene lake development in glaciated regions. *Journal of Paleolimnology*, *49*(3), 349-362.

Frugone-Álvarez, M., Latorre, C., Barreiro-Lostres, F., Giralt, S., Moreno, A., Polanco-Martínez, J., ... & Valero-Garcés, B. (2020). Volcanism and climate change as drivers in Holocene depositional dynamic of Laguna del Maule (Andes of central Chile–36° S). *Climate of the Past*, *16*(4), 1097-1125.

García, M. L., Maidana, N. I., Ector, L., & Morales, E. A. (2018). Staurosira patagonica sp. nov., a new diatom (Bacillariophyta) from southern Argentina, with a discussion on the genus Staurosira Ehrenberg. *Nova Hedwigia, Beihefte*, 103-123.

García, M. L., Morales, E. A., Guerrero, J. M., Tremarin, P. I., & Maidana, N. I. (2019). New Aulacoseira species (Bacillariophyta) from the Argentinean Patagonia and re-examination of type material of Melosira perpusilla Frenguelli. *Phytotaxa*, *408*(3), 161-177.

García, M. L., Morales, E. A., Mann, D. G., & Maidana, N. I. (2020). Sellaphora mayrii (Bacillariophyceae), a new diatom from the Argentinean Patagonia. *Phytotaxa*, *437*(3), 135-146.

García, M. L., Bustos, S., Villacís, L. A., Laprida, C., Mayr, C., Moreno, P. I., ... & Morales, E. A. (2021). New araphid species of the genus Pseudostaurosira (Bacillariophyceae) from southern Patagonia. *European Journal of Phycology*, 1-18.

Garreaud, R. (2007). Precipitation and circulation covariability in the extratropics. *Journal of Climate*, *20*(18), 4789-4797.

Garreaud, R. D., Vuille, M., Compagnucci, R., & Marengo, J. (2009). Present-day south american climate. *Palaeogeography, Palaeoclimatology, Palaeoecology*, *281*(3-4), 180-195.

Garreaud, R., Lopez, P., Minvielle, M., & Rojas, M. (2013). Large-scale control on the Patagonian climate. *Journal of Climate*, *26*(1), 215-230.

Genkal, S. I., & Kulikovskiy, M. S. (2014). Centric diatoms from Lake Frolikha (Transbaikal area) and peculiarities of distribution of some taxa in Asia. *Inland water biology*, *7*(3), 201-210.

Gomez, B., Carter, L., Orpin, A. R., Cobb, K. M., Page, M. J., Trustrum, N. A., & Palmer, A. S. (2012). ENSO/SAM interactions during the middle and late Holocene. *The Holocene*, *22*(1), 23-30.

Gong, D., & Wang, S. (1999). Definition of Antarctic oscillation index. *Geophysical research letters*, *26*(4), 459-462.

Grimm, E. C. (1987). CONISS: a FORTRAN 77 program for stratigraphically constrained cluster analysis by the method of incremental sum of squares. *Computers & geosciences*, *13*(1), 13-35.

Guerrero, J. M., García, M. L., & Morales, E. A. (2019). Staurosirella andino-patagonica sp. nov.(Bacillariophyta) from lake sediments in Patagonia, Argentina. *Phytotaxa*, *402*(3), 131-144.

Hasle, G. R., & Fryxell, G. A. (1970). Diatoms: cleaning and mounting for light and electron microscopy. *Transactions of the American Microscopical Society*, 469-474.

Haug, G. H., Hughen, K. A., Sigman, D. M., Peterson, L. C., & Röhl, U. (2001). Southward migration of the intertropical convergence zone through the Holocene. *Science*, *293*(5533), 1304-1308.

Henríquez, C. A., Moreno, P. I., Lambert, F., & Alloway, B. V. (2021). The role of climate and disturbance regimes upon temperate rainforests during the Holocene: A stratigraphic perspective from Lago Fonk (∼ 40° S), northwestern Patagonia. *Quaternary Science Reviews*, *258*, 106890.

Heusser, C. J. (1995). Three Late Quaternary pollen diagrams from Southern Patagonia and their palaeoecological implications. *Palaeogeography, Palaeoclimatology, Palaeoecology*, *118*(1-2), 1-24.

Hodgson, D. A., & Sime, L. C. (2010). Southern westerlies and CO 2. *Nature Geoscience*, *3*(10), 666-667.

Hofmann, G., Werum, M., & Lange-Bertalot, H. (2011). *Diatomeen im Süßwasser-Benthos von Mitteleuropa: Bestimmungsflora Kieselalgen für die ökologische Praxis; über 700 der häufigsten Arten und ihrer Ökologie*. Gantner.

Hogg, A. G., Heaton, T. J., Hua, Q., Palmer, J. G., Turney, C. S., Southon, J., ... & Wacker, L. (2020). SHCal20 Southern Hemisphere calibration, 0–55,000 years cal BP. *Radiocarbon*, *62*(4), 759-778.

Huber, U. M., & Markgraf, V. (2003). Holocene fire frequency and climate change at Rio Rubens Bog, southern Patagonia. In *Fire and climatic change in temperate ecosystems of the western Americas* (pp. 357-380). Springer, New York, NY.

Jara, I. A., & Moreno, P. I. (2014). Climatic and disturbance influences on the temperate rainforests of northwestern Patagonia (40° S) since∼ 14,500 cal yr BP. *Quaternary Science Reviews*, *90*, 217-228.

Jara, I. A., Newnham, R. M., Vandergoes, M. J., Foster, C. R., Lowe, D. J., Wilmshurst, J. M., ... & Homes, A. M. (2015). Pollen–climate reconstruction from northern South Island, New Zealand (41° S), reveals varying high-and low-latitude teleconnections over the last 16 000 years. *Journal of Quaternary Science*, *30*(8), 817-829.

Jenny, B., Wilhelm, D., & Valero-Garcés, B. (2003). The Southern Westerlies in Central Chile: Holocene precipitation estimates based on a water balance model for Laguna Aculeo (33 50' S). *Climate Dynamics*, *20*(2-3), 269-280.

Juggins, S., & Juggins, M. S. (2020). Package 'rioja'.

Kaplan, M. R., Strelin, J. A., Schaefer, J. M., Peltier, C., Martini, M. A., Flores, E., ... & Schwartz, R. (2020). Holocene glacier behavior around the northern Antarctic Peninsula and possible causes. *Earth and Planetary Science Letters*, *534*, 116077.

Kilian, R., Baeza, O., Steinke, T., Arevalo, M., Rios, C., & Schneider, C. (2007). Late Pleistocene to Holocene marine transgression and thermohaline control on sediment transport in the western Magellanes fjord system of Chile (53 S). *Quaternary International*, *161*(1), 90-107.

Kilian, R., Schneider, C., Koch, J., Fesq-Martin, M., Biester, H., Casassa, G., ... & Behrmann, J. (2007). Palaeoecological constraints on late Glacial and Holocene ice retreat in the Southern Andes (53 S). *Global and Planetary Change*, *59*(1-4), 49-66.

Kilian, R., & Lamy, F. (2012). A review of Glacial and Holocene paleoclimate records from southernmost Patagonia (49–55 S). *Quaternary Science Reviews*, *53*, 1-23.

Krammer, K. (1991). Suβwasserflora von Mitteleuropa. Bacillariophyceae. 3. Teil: Centrales, Fragilariaceae, Eunotiaceae. *Sußwasserflora von Mitteleuropa*.

Krammer, K. (1997). Die cymbelloiden diatomeen. Eine monographie der weltweit bekannten Taxa. Teil 1. Allgemeines und Encyonema part. *Bibliotheca diatomol*, *36*, 1-382.

Krammer, K. (2000). Diatoms of Europe. Diatoms of the European Inland Waters and Comparable Habitats, Vol. 1. The genus Pinnularia. *Ruggell, Liechtenstein: ARG Gantner Verlag*.

Krammer, K. (2003). Diatoms of Europe, vol. 4: Cymbopleura, Delicata, Navicymbella, Gomphocymbellopsis, Afrocymbella. ARG Gantner Verlag, Ruggell . 530 pp.

Kramer, K., & Lange-Bertalot, H. (1986). Bacillariophyceae. 1. Teil: Naviculaceae. Süsswasserflora von Mitteleuropa. Band 2/1.

Krammer, K., & Lange-Bertalot, H. (1988). Bacillariophyceae, Teil 2: Epithemiaceae, Bacillariaceae, Surirellaceae. *Süsswasserflora von Mitteleuropa, Bd*, *2*(2).

Laing, T. E., & Smol, J. P. (2003). Late Holocene environmental changes inferred from diatoms in a lake on the western Taimyr Peninsula, northern Russia. *Journal of Paleolimnology*, *30*(2), 231-247.

Lambert, F., Delmonte, B., Petit, J. R., Bigler, M., Kaufmann, P. R., Hutterli, M. A., ... & Maggi, V. (2008). Dust-climate couplings over the past 800,000 years from the EPICA Dome C ice core. *Nature*, *452*(7187), 616-619.

Lamy, F., Kilian, R., Arz, H. W., Francois, J. P., Kaiser, J., Prange, M., & Steinke, T. (2010). Holocene changes in the position and intensity of the southern westerly wind belt. *Nature Geoscience*, *3*(10), 695-699.

Lamy, F., Arz, H. W., Kilian, R., Lange, C. B., Lembke-Jene, L., Wengler, M., ... & Tiedemann, R. (2015). Glacial reduction and millennial-scale variations in Drake Passage throughflow. *Proceedings of the National Academy of Sciences*, *112*(44), 13496-13501.

Lange-Bertalot, H. (1994). Brachysira. Monographie der Gattung. Wichtige Indikator-Species fur das Gewasser-Monitoring und Naviculadicta nov. gen. Ein Losungsvorschlag zu dem Problem Navicula sensu lato ohne Navicula sensu stricto. *Bibliotheca. Diatomologica*, *29*, 1-212.

Lange-Bertalot, H. (1996). Diatom taxa introduced by Georg Krasske documentation and revision. *Iconographia Diatomologica*, *3*, 1-358.

Lange-Bertalot, H. (2001). Diatoms of the European inland waters and comparable habitats. Navicula sensu stricto. 10 genus separated from Navicula sensu lato. Frustulia. Diatoms of Europe 2.4

Lange-Bertalot, H., & Krammer, K. (1989). Achnanthes, eine monographie der gattung.

Lange-Bertalot, H., Bąk, M., Witkowski, A., & Tagliaventi, N. (2011). Diatoms of the European inland waters and comparable habitats, Eunotia and some related genera. *Diatoms of Europe*, *6*.

Lara, A., Donoso, C., Escobar, B., Rovere, A., Premoli, A., Soto, D. P., & Bannister, J. (2006). Pilgerodendron uviferum (D. Don) florin. *Las especies arbóreas de los bosques templados de Chile y Argentina, Autoecología*, 82-91.

Latorre, C., De Pol-Holz, R., Carter, C., & Santoro, C. M. (2017). Using archaeological shell middens as a proxy for past local coastal upwelling in northern Chile. *Quaternary International*, *427*, 128-136.

Lotter, André F., and Christian Bigler. "Do diatoms in the Swiss Alps reflect the length of ice-cover?." *Aquatic sciences* 62.2 (2000): 125-141.

Lundström, U. S., van Breemen, N., & Bain, D. (2000). The podzolization process. A review. *Geoderma*, *94*(2-4), 91-107.

Mann, D. G., McDonald, S. M., Bayer, M. M., Droop, S. J., Chepurnov, V. A., Loke, R. E., ... & Du Buf, J. H. (2004). The Sellaphora pupula species complex (Bacillariophyceae): morphometric analysis, ultrastructure and mating data provide evidence for five new species. *Phycologia*, *43*(4), 459-482.

Marden, C. J. (1997). Late-glacial fluctuations of South Patagonian Icefield, Torres del Paine National Park, southern Chile. *Quaternary International*, *38*, 61-68.

Martínez Fontaine, C., De Pol-Holz, R., Michel, E., Siani, G., Reyes-Macaya, D., Martínez-Méndez, G., ... & Hebbeln, D. (2019). Ventilation of the deep ocean carbon reservoir during the last deglaciation: results from the southeast pacific. *Paleoceanography and Paleoclimatology*, *34*(12), 2080-2097.

Massaferro, J., Recasens, C., Larocque-Tobler, I., Zolitschka, B., & Maidana, N. I. (2013). Major lake level fluctuations and climate changes for the past 16,000 years as reflected by diatoms and chironomids preserved in the sediment of Laguna Potrok Aike, southern Patagonia. *Quaternary Science Reviews*, *71*, 167-174.

Mayr, C., Smith, R. E., García, M. L., Massaferro, J., Lücke, A., Dubois, N., ... & Zolitschka, B. (2019). Historical eruptions of Lautaro Volcano and their impacts on lacustrine ecosystems in southern Argentina. *Journal of paleolimnology*, *62*(2), 205-221.

McCulloch, R. D., & Davies, S. J. (2001). Late-glacial and Holocene palaeoenvironmental change in the central Strait of Magellan, southern Patagonia. *Palaeogeography, Palaeoclimatology, Palaeoecology*, *173*(3-4), 143-173.

McCulloch, R. D., Fogwill, C. J., Sugden, D. E., Bentley, M. J., & Kubik, P. W. (2005). Chronology of the last glaciation in central Strait of Magellan and Bahía Inútil, southernmost South America. *Geografiska Annaler: Series A, Physical Geography*, *87*(2), 289-312.

McCulloch, R. D., Blaikie, J., Jacob, B., Mansilla, C. A., Morello, F., De Pol-Holz, R., ... & Torres, J. (2020). Late glacial and Holocene climate variability, southernmost Patagonia. *Quaternary Science Reviews*, *229*, 106131.

Monnin, E., Indermühle, A., Dällenbach, A., Flückiger, J., Stauffer, B., Stocker, T. F., ... & Barnola, J. M. (2001). Atmospheric CO2 concentrations over the last glacial termination. *science*, *291*(5501), 112-114.

Moreno, P. I. (2002). Western Patagonia: a key area for understanding Quaternary paleoclimate at southern mid-latitudes. In *The Patagonian Icefields* (pp. 43-54). Springer, Boston, MA.

Moreno, P. I., François, J. P., Villa-Martínez, R. P., & Moy, C. M. (2009). Millennial-scale variability in Southern Hemisphere westerly wind activity over the last 5000 years in SW Patagonia. *Quaternary Science Reviews*, *28*(1-2), 25-38.

Moreno, P. I., Kaplan, M. R., François, J. P., Villa-Martínez, R., Moy, C. M., Stern, C. R., & Kubik, P. W. (2009). Renewed glacial activity during the Antarctic cold reversal and persistence of cold conditions until 11.5 ka in southwestern Patagonia. *Geology*, *37*(4), 375-378.

Moreno, P. I., Francois, J. P., Moy, C. M., & Villa-Martínez, R. (2010). Covariability of the Southern Westerlies and atmospheric CO2 during the Holocene. *Geology*, *38*(8), 727-730.

Moreno, P. I., Villa-Martínez, R., Cárdenas, M. L., & Sagredo, E. A. (2012). Deglacial changes of the southern margin of the southern westerly winds revealed by terrestrial records from SW Patagonia (52 S). *Quaternary Science Reviews*, *41*, 1-21.

Moreno, P. I., & Videla, J. (2016). Centennial and millennial-scale hydroclimate changes in northwestern Patagonia since 16,000 yr BP. *Quaternary Science Reviews*, *149*, 326-337.

Moreno, P. I., Videla, J., Valero-Garcés, B., Alloway, B. V., & Heusser, L. E. (2018). A continuous record of vegetation, fire-regime and climatic changes in northwestern Patagonia spanning the last 25,000 years. *Quaternary Science Reviews*, *198*, 15-36.

Moreno, P. I., Vilanova, I., Villa-Martínez, R. P., & Francois, J. P. (2018). Modulation of fire regimes by vegetation and site type in southwestern Patagonia since 13 ka. *Frontiers in Ecology and Evolution*, *6*, 34.

Moreno, P. I., Vilanova, I., Villa-Martínez, R., Dunbar, R. B., Mucciarone, D. A., Kaplan, M. R., ... & Lambert, F. (2018). Onset and evolution of southern annular mode-like changes at centennial timescale. *Scientific Reports*, *8*(1), 1-9.

Moreno, P. I., Henríquez, W. I., Pesce, O. H., Henríquez, C. A., Fletcher, M. S., Garreaud, R. D., & Villa-Martínez, R. P. (2021). An early Holocene westerly minimum in the southern mid-latitudes. *Quaternary Science Reviews*, *251*, 106730.

Mottl, O., Grytes, J. A., Seddon, A. W., Steinbauer, M. J., Bhatta, K. P., Felde, V. A., ... & Birks, H. J. B. (2021). Rate-of-change analysis in palaeoecology revisited: a new approach. *bioRxiv*, 2020-12.

Moy, C. M., Seltzer, G. O., Rodbell, D. T., & Anderson, D. M. (2002). Variability of El Niño/Southern Oscillation activity at millennial timescales during the Holocene epoch. *Nature*, *420*(6912), 162-165.

Moy, C. M., Dunbar, R. B., Moreno, P. I., Francois, J. P., Villa-Martínez, R., Mucciarone, D. M., ... & Garreaud, R. D. (2008). Isotopic evidence for hydrologic change related to the westerlies in SW Patagonia, Chile, during the last millennium. *Quaternary Science Reviews*, *27*(13-14), 1335-1349.

Moy, C. M., Dunbar, R. B., Guilderson, T. P., Waldmann, N., Mucciarone, D. A., Recasens, C., ... & Anselmetti, F. S. (2011). A geochemical and sedimentary record of high southern latitude Holocene climate evolution from Lago Fagnano, Tierra del Fuego. *Earth and planetary science letters*, *302*(1-2), 1-13.

Mulvaney, R., Abram, N. J., Hindmarsh, R. C., Arrowsmith, C., Fleet, L., Triest, J., ... & Foord, S. (2012). Recent Antarctic Peninsula warming relative to Holocene climate and ice-shelf history. *Nature*, *489*(7414), 141-144.

Neil, K., & Lacourse, T. (2019). Diatom responses to long-term climate and sea-level rise at a low-elevation lake in coastal British Columbia, Canada. *Ecosphere*, *10*(9), e02868.

Overpeck, J. T., Webb III, T., & Prentice, I. C. (1985). Quantitative interpretation of fossil pollen spectra: dissimilarity coefficients and the method of modern analogs. *Quaternary Research*, *23*(1), 87-108.

Pedro, J. B., Bostock, H. C., Bitz, C. M., He, F., Vandergoes, M. J., Steig, E. J., ... & Cortese, G. (2016). The spatial extent and dynamics of the Antarctic Cold Reversal. *Nature Geoscience*, *9*(1), 51-55.

Pesce, O. H., & Moreno, P. I. (2014). Vegetation, fire and climate change in central-east Isla Grande de Chiloé (43 S) since the Last Glacial Maximum, northwestern Patagonia. *Quaternary Science Reviews*, *90*, 143-157.

Pisano Valdés, E. (1992). Sectorización fitogeográfica del archipielago sud patagónico-fueguino. V: Sintaxonomía y distribución de las unidades de vegetación vascular. In *Anales del Instituto de la Patagonia*.

Quade, J., & Kaplan, M. R. (2017). Lake-level stratigraphy and geochronology revisited at Lago (Lake) Cardiel, Argentina, and changes in the Southern Hemispheric Westerlies over the last 25 ka. *Quaternary Science Reviews*, *177*, 173-188.

Recasens, C., Ariztegui, D., Maidana, N. I., Zolitschka, B., & Team, P. S. (2015). Diatoms as indicators of hydrological and climatic changes in Laguna Potrok Aike (Patagonia) since the Late Pleistocene. *Palaeogeography, Palaeoclimatology, Palaeoecology*, *417*, 309-319.

Reichardt, E. (2015). Gomphonema gracile Ehrenberg sensu stricto et sensu auct.(Bacillariophyceae): A taxonomic revision. *Nova Hedwigia*, 367-393.

Reynhout, S. A., Sagredo, E. A., Kaplan, M. R., Aravena, J. C., Martini, M. A., Moreno, P. I., ... & Schaefer, J. M. (2019). Holocene glacier fluctuations in Patagonia are modulated by summer insolation intensity and paced by Southern Annular Mode-like variability. *Quaternary Science Reviews*, *220*, 178-187.

Ríos, F., Kilian, R., Lange, C. B., Baeza-Urrea, O., Arz, H. W., Zindorf, M., ... & Lamy, F. (2020). Environmental and coastline changes controlling Holocene carbon accumulation rates in fjords of the western Strait of Magellan region. *Continental Shelf Research*, *199*, 104101.

Rodionov, S. N. (2004). A sequential algorithm for testing climate regime shifts. *Geophysical Research Letters*, *31*(9).

Rumrich, U. (2000). Diatomeen der Anden. Von Venezuela bis Patagonien/Feuerland. *Iconographia diatomologica*, *9*, 673.

Rühland, K. M., Paterson, A. M., & Smol, J. P. (2015). Lake diatom responses to warming: reviewing the evidence. *Journal of paleolimnology*, *54*(1), 1-35.

Sagredo, E. A., Moreno, P. I., Villa-Martínez, R., Kaplan, M. R., Kubik, P. W., & Stern, C. R. (2011). Fluctuations of the Última Esperanza ice lobe (52 S), Chilean Patagonia, during the last glacial maximum and termination 1. *Geomorphology*, *125*(1), 92-108.

Sala, S. E., & Ramírez, J. J. (2008). Diatoms from lentic and lotic systems in Antioquia, Chocó and Santander Departments in Colombia. *Revista de biología tropical*, *56*(3), 1159-1178.

Schmitt, J., Schneider, R., Elsig, J., Leuenberger, D., Lourantou, A., Chappellaz, J., ... & Fischer, H. (2012). Carbon isotope constraints on the deglacial CO2 rise from ice cores. *Science*, *336*(6082), 711-714.

Schneider, C., Glaser, M., Kilian, R., Santana, A., Butorovic, N., & Casassa, G. (2003). Weather observations across the southern Andes at 53 S. *Physical Geography*, *24*(2), 97-119.

Schneider, C., & Gies, D. (2004). Effects of El Niño–southern oscillation on southernmost South America precipitation at 53 S revealed from NCEP–NCAR reanalyses and weather station data. *International Journal of Climatology: A Journal of the Royal Meteorological Society*, *24*(9), 1057-1076.

Shevenell, A. E., Ingalls, A. E., Domack, E. W., & Kelly, C. (2011). Holocene Southern Ocean surface temperature variability west of the Antarctic Peninsula. *Nature*, *470*(7333), 250-254.

Simpson, G. L. (2007). Analogue methods in palaeoecology: using the analogue package. *Journal of Statistical Software*, *22*(2), 1-29.

Siver, P. A., & Kling, H. (1997). Morphological observations of Aulacoseira using scanning electron microscopy. *Canadian journal of botany*, *75*(11), 1807-1835.

Smol, J. P., & Cumming, B. F. (2000). Tracking long-term changes in climate using algal indicators in lake sediments. *Journal of Phycology*, *36*(6), 986-1011.

Smol, J. P., & Douglas, M. S. (2007). From controversy to consensus: making the case for recent climate change in the Arctic using lake sediments. *Frontiers in Ecology and the Environment*, *5*(9), 466-474.

Smol, J. P., & Stoermer, E. F. (Eds.). (2010). *The diatoms: applications for the environmental and earth sciences*. Cambridge University Press.

Schrader, H., & Gersonde, R. (1978). Diatoms and silicoflagellates. *In Zachariasse etb al. Microplaeontological counting methods and techniques-an excercise on an eight metres section of the lower Pliocene of Capo Rossello. Sicily. Utrecht Micropal. Bull. 17:*, 129-176.

Stevenson, A. C., Juggins, S., Birks, H. J. B., Anderson, D. S., Anderson, N. J., Battarbee, R. W., ... & Renberg, I. (1991). *The surface waters acidification project palaeolimnology programme: modern diatom/lake-water chemistry data-set*. UCL Environmental Change Research Centre.

Toggweiler, J. R., Russell, J. L., & Carson, S. R. (2006). Midlatitude westerlies, atmospheric CO2, and climate change during the ice ages. *Paleoceanography*, *21*(2).

Toggweiler, J. R. (2009). Shifting westerlies. *Science*, *323*(5920), 1434-1435.

Trifonova, I., & Genkal, S. (2001, August). Species of the genus Aulacoseira Thwaites in lakes and rivers of north-western Russia-distribution and ecology. In *Proceedings of the 16th International Diatom Symposium, Athens and Aegean Islands* (Vol. 25, pp. 315-322). Athens: Univ. of Athens.

Unkel, I., Fernandez, M., Björck, S., Ljung, K., & Wohlfarth, B. (2010). Records of environmental changes during the Holocene from Isla de los Estados (54.4 S), southeastern Tierra del Fuego. *Global and Planetary Change*, *74*(3-4), 99-113.

Valero-Garcés, B. L., Jenny, B., Rondanelli, M., Delgado-Huertas, A., Burns, S. J., Veit, H., & Moreno, A. (2005). Palaeohydrology of Laguna de Tagua (34 30' S) and moisture fluctuations in Central Chile for the last 46 000 yr. *Journal of Quaternary Science: Published for the Quaternary Research Association*, *20*(7-8), 625-641.

Van de Vijver, B., Frenot, Y., & Beyens, L. (2002). Freshwater diatoms from Ile de la Possession (Crozet-Archipelago, Subantarctica). *Acta Botanica Ungarica*, *45*(3-4), 422-423.

Van de Vijver, B., Beyens, L., & Lange-Bertalot, H. (2004). The genus Stauroneis in the Arctic and (sub-) Antarctic-regions.

Vermaire, J. C., & Gregory-Eaves, I. (2008). Reconstructing changes in macrophyte cover in lakes across the northeastern United States based on sedimentary diatom assemblages. *Journal of paleolimnology*, *39*(4), 477-490.

Villa-Martínez, R., & Moreno, P. I. (2007). Pollen evidence for variations in the southern margin of the westerly winds in SW Patagonia over the last 12,600 years. *Quaternary Research*, *68*(3), 400-409.

Wetzel, C. E., Ector, L., Van de Vijver, B., Compère, P., & Mann, D. G. (2015). Morphology, typification and critical analysis of some ecologically important small naviculoid species (Bacillariophyta). *Fottea*, *15*(2), 203-234.

Wille, M., Maidana, N. I., Schäbitz, F., Fey, M., Haberzettl, T., Janssen, S., ... & Zolitschka, B. (2007). Vegetation and climate dynamics in southern South America: the microfossil record of Laguna Potrok Aike, Santa Cruz, Argentina. *Review of Palaeobotany and Palynology*, *146*(1-4), 234-246.

Wille, M., & Schäbitz, F. (2009). Late-glacial and Holocene climate dynamics at the steppe/forest ecotone in southernmost Patagonia, Argentina: the pollen record from a fen near Brazo Sur, Lago Argentino. *Vegetation History and Archaeobotany*, *18*(3), 225-234.

Wiltse, B., Paterson, A. M., Findlay, D. L., & Cumming, B. F. (2016). Seasonal and decadal patterns in Discostella (Bacillariophyceae) species from bi-weekly records of two boreal lakes (Experimental Lakes Area, Ontario, Canada). *Journal of phycology*, *52*(5), 817-826.

Whitlock, C., Moreno, P. I., & Bartlein, P. (2007). Climatic controls of Holocene fire patterns in southern South America. *Quaternary Research*, *68*(1), 28-36.

Wolfe, A. P. (1997). On diatom concentrations in lake sediments: results from an inter-laboratory comparison and other tests performed on a uniform sample. *Journal of Paleolimnology*, *18*(3), 261-268.

SUPPLEMENTARY MATERIAL

Binary functional group assignation of each taxon

Table SI. Listing of identified diatom species and corresponding functional groups.

#	Species name	code	Sub-Antarctic?	plankton	*Aulacoseira*	small fragilarioid	NFB
1	*Achnanthidium aff. modestiformis* (Lange-Bertalot) Van de Vijver	PSAC001	1	0	0	0	1
2	*Achnanthidium aff. sieminskae* Witkowski, Kulikovsky & Riaux-gobin	PSAC002	0	0	0	0	1
3	*Achnanthidium exiguum var angustirostrata* (Krasske) Echazú & Maidana	PLAC003	1	0	0	0	1
4	Achnanthidium sp2	PSAC004	?	0	0	0	1
5	*Achnanthidium spp. cf. minutissimum* Kützing sensu lato	PSAC005	?	0	0	0	1
6	*Adlafia sp*	PSAD006	?	0	0	0	1
7	*aff Eolimna* (?nov) spec. sensu Rumrich 2000	PSEO007	?	0	0	0	1
8	*Amphipleura pellucida* (Kützing) Kützing	PLAM008	0	0	0	0	1
9	*Amphora copulata* (Kützing) Schoeman & Archibald	PLAM009	0	0	0	0	1
10	*Amphora sp.1*	PSAM010	?	0	0	0	1
11	*Aulacoseira aff. distans* (Ehrenberg) Simonsen	CSAU011	?	0	1	0	0
12	*Aulacoseira aff. lacustris* (Grunow) Krammer	CLAU012	?	0	1	0	0
13	*Aulacoseira humilis* (Cleve-Euler) Genkal et Trifonova	CSAU013	?	0	1	0	0
14	*Aulacoseira lauquenensis* M.L. García, J.M. Guerrero, Tremarin, Maidana & Morales	CSAU014	1	0	1	0	0
15	*Aulacoseira liucoensis* M.L. García, J.M. Guerrero, Tremarin, Maidana & Morales	CSAU015	1	0	1	0	0
16	*Aulacoseira subarctica* (O. Muller) Haworth	CLAU016	0	0	1	0	0
17	*Brachysira aff. aponina* Kützing	PLBR017	0	0	0	0	1
18	*Brachysira aff. brebisonii* (Brébisson) R. Ross	PLBR018	0	0	0	0	1
19	*Brachysira aff. microcephala* (Grunow) Compère	PLBR019	0	0	0	0	1
20	*Caloneis bacillum* (Grunow) Cleve	PLCA020	0	0	0	0	1
21	*Caloneis silicula* (Ehrenberg) Cleve	PLCA021	0	0	0	0	1
22	*Caloneis sp1*	PLCA022	?	0	0	0	1
23	*Cavinula pseudoscutiformis* (Grunow) Mann & Stickle	PLCA023	0	0	0	0	1
24	*Cocconeis sp1*	PSCO024	?	0	0	0	1
25	*Craticula acidoclinata* Lange-Bertalot & Metzeltin	PLCR025	0	0	0	0	1
26	*Craticula halophila* (Grunow) Mann	PLCR026	0	0	0	0	1
27	*Cymbella aff. subantartica* Krammer	HLCY027	?	0	0	0	1
28	*Cymbella peranglica* Krammer	HLCY028	0	0	0	0	1
29	*Cymbella peraspera* Krammer	HLCY029	0	0	0	0	1
30	*Cymbella simonsenii* Krammer	HLCY030	0	0	0	0	1
31	*Cymbopleura aff. tsoneka* Lange-Bertalot, Krammer & Rumrich	HLCY031	1	0	0	0	1

32	*Cymbopleura sp* aff. ehrenbergii	HLCY032	0	0	0	0	1
33	*Denticula kuetzingii* Grunow	PLDE033	0	0	0	0	1
34	*Diatomella balfouriana* (W. Smith) Grev.	PSDI034	0	0	0	0	1
35	*Diploneis krammeri* Lange-Bertalot & E. Reichardt	PLDI035	0	0	0	0	1
36	*Diploneis sp.1*	PLDI036	?	0	0	0	1
37	*Diploneis subovalis* Cleve	PLDI037	0	0	0	0	1
38	*Discostella pseudostelligera* (Hustedt) Houk et Klee	CLDI038	0	1	0	0	0
39	*Distrionella coxiana* Casa & Van de Vijver	PLDI039	1	1	0	0	0
40	*Encyonema aff. dificilima* Krammer	HLEN040	?	0	0	0	1
41	*Encyonema aff. jentlandicum* Krammer	HLEN041	?	0	0	0	1
42	*Encyonema aff. silesiacum* (Bleisch) Mann	HLEN042	?	0	0	0	1
43	*Encyonema aff. subtriste* Krammer	HLEN043	?	0	0	0	1
44	*Encyonema lancettulum* Krammer	HLEN044	0	0	0	0	1
45	*Encyonema neogracile* Krammer	HLEN045	0	0	0	0	1
46	*Encyonopsis aff.* "patagonensis" Echazú & Maidana	HSEN046	1	0	0	0	1
47	*Encyonopsis microcephala* (Grunow) Krammer	HSEN047	0	0	0	0	1
48	*Encyonopsis rumrichae* Krammer	HSEN048	0	0	0	0	1
49	*Encyonopsis subminuta* Krammer & Reichardt	HSEN049	0	0	0	0	1
50	*Eolimna minima* (Grunow) Lange-bertalot sensu Van de Vijver	PSEO050	?	0	0	0	1
51	*Epithemia adnata* (Kützing) Brébisson	HLEP051	0	0	0	0	1
52	*Epithemia argus* (Ehrenberg) Kützing	HLEP052	0	0	0	0	1
53	*Eunotia sp1*	HLEU053	?	0	0	0	1
54	*Eunotia aff. arcus* Ehrenberg	HLEU054	?	0	0	0	1
55	*Eunotia aff. incisa* W. Smith ex W. Gregory	HSEU055	?	0	0	0	1
56	*Eunotia aff. naegellii* Migula	HLEU056	?	0	0	0	1
57	*Eunotia aff. suecica* A. Cleve 1895	HLEU057	?	0	0	0	1
58	*Eunotia aff. vanheurckii* Patrick	HSEU058	?	0	0	0	1
59	*Eunotia ambivalens* Lange-Bertalot & Togliaventi	HLEU059	0	0	0	0	1
60	*Eunotia glacialis* Meister 1912	HLEU060	0	0	0	0	1
61	*Eunotia implicata* Nörpel-Schempp, Alles & Lange-Bertalot	HSEU061	0	0	0	0	1
62	*Eunotia sp2*	HSEU062	?	0	0	0	1
63	*Eunotia metamonodon* Lange-Bertalot	HLEU063	0	0	0	0	1
64	*Eunotia sp3*	HLEU064	?	0	0	0	1
65	*Eunotia sp aff. pectinalis (*Kützing) Rabenhorst	HLEU065	?	0	0	0	1
66	*Eunotia tridentata* (Ehrenbeg) Frenguelli	HLEU066	1	0	0	0	1
67	*Fragilaria aff. amphicephaloides* Lange-Bertalot	FLFR067	?	1	0	0	0
68	*Fragilaria aff. delicatissima* (W. Smith) Lange-Bertalot	FLFR068	?	1	0	0	0
69	*Fragilaria aff. vaucheriae* (Kützing) J.B. Peterson	FLFR069	?	1	0	0	0
70	*Frustulia krammeri* Lange-Bertalot & Metzeltin	PLFR070	0	0	0	0	1
71	*Frustulia saxonica* Rabenhorst	PLFR071	0	0	0	0	1

72	*Frustulia sp1*	PLFR072	?	0	0	0	1
73	*Gomphonema sp1*	PLGO073	?	0	0	0	1
74	*Gomphonema aff. lagenula* Kützing	PLGO074	?	0	0	0	1
75	*Gomphonema aff. possessionense* Van de Vijver & Beyens	PSGO075	1	0	0	0	1
76	*Gomphonema aff. pumilum* (Grunow) Reichardt & Lange-Bertalot 1991	PSGO076	?	0	0	0	1
77	*Gomphonema anglicum* Ehrenberg	PLGO077	0	0	0	0	1
78	*Gomphonema auritum* A. Braun ex Kützing 1849	PSGO078	0	0	0	0	1
79	*Gomphonema cf. exilissimum* (Grunow) Lange-Bertalot & Reichardt 1996	PSGO079	?	0	0	0	1
80	*Gomphonema hebridense* Gregory	PLGO080	0	0	0	0	1
81	*Gomphonema lagenula* Kützing	PLGO081	0	0	0	0	1
82	*Gomphonema patagonicum* Krasske 1939	PLGO082	1	0	0	0	1
83	*Gyrosigma aff. nodiferum* (Grunow) Reimer 1966	PLGY083	?	0	0	0	1
84	*Hantzschia sp1*	PLHA084	?	0	0	0	1
85	*Humidophila schmassmanni* (Hustedt) Kuczkó and Wojtal 2015	PSHU085	0	0	0	0	1
86	*Iconella aff. delicatissima* (Lewis) Ruck & Nakov	PLIC086	?	0	0	0	1
87	*Iconella guatimalensis* (Ehrenberg) Ruck & Nakov	PLIC087	0	0	0	0	1
88	*Adlafia aff. minuscula*(Grunow) Lange-Bertalot	PSXX088	?	0	0	0	1
89	*Karayevia clevei* (Grunow) Bukhtiyarova	PLKA089	0	0	0	0	1
90	*Karayevia oblongella* (Oestrup) Aboal	PLKA090	0	0	0	0	1
91	*Meridion circulare* (Greville) C. Agardh	PLME091	0	0	0	0	1
92	*Microcostatus* sp1	PSMI092	?	0	0	0	1
93	*Navicula aff. difficillima* Hustedt	PLNA093	?	0	0	0	1
94	*Navicula aff. radiosa* Kützing	PLNA094	?	0	0	0	1
95	*Navicula angusta* Grunow	PLNA095	0	0	0	0	1
96	*Navicula mirifica var. 2* (?nov var)	PLNA096	1	0	0	0	1
97	*Navicula mirifica var.lanceolata* Krasske	PLNA097	1	0	0	0	1
98	*Navicula radiosa* Kützing	PLNA098	0	0	0	0	1
99	*Navicula rhynchocephala* Kützing sensu stricto	PLNA099	0	0	0	0	1
100	*Navicula subalpina* Reichardt	PLNA100	0	0	0	0	1
101	*Naviculadicta seminulum* (Grunow) Van de Vijver 2002	PSNA101	1	0	0	0	1
102	*Neidiomorpha binodiformis* (Krammer) Cantonati, Lange-Bertalot & Angeli	PLNE102	0	0	0	0	1
103	*Neidium ampliatum* (Ehrenberg) Krammer	PLNE103	0	0	0	0	1
104	*Neidium magellanicum var. minor* (Frenguelli) F.W. Mills	PLNE104	1	0	0	0	1
105	*Neidium sp.* 1	PLNE105	?	0	0	0	1
106	*Nitzschia fonticola* Grunow	PSNI106	0	0	0	0	1
107	*Nitzschia oberheimiana* Rumrich & Lange-Bertalot	PSNI107	1	0	0	0	1
108	*Nitzschia inconspicua* Grunow	PSNI108	0	0	0	0	1
109	*Nitzschia palea* (Kützing) W. Smith	PSNI109	0	0	0	0	1
110	*Nitzschia* sp1	PLNI110	?	0	0	0	1

111	*Nupela lapidosa* (Krasske) Lange-Bertalot	PLNU111	0	0	0	0	1
112	*Orthoseira sp*	CLOR112	?	1	0	0	0
113	*Pinnularia acrosphaeria* W. Smith 1853	PLPI113	0	0	0	0	1
114	*Pinnularia aff. gigas* Ehrenberg 1843	PLPI114	?	0	0	0	1
115	*Pinnularia aff. inconstans* Mayer	PLPI115	?	0	0	0	1
116	*Pinnularia aff. interrumpiformis* Krammer	PLPI116	?	0	0	0	1
117	*Pinnularia borealis* Ehrenberg	PLPI117	0	0	0	0	1
118	*Pinnularia divergens var bacillaris* (M. Peragallo) Mills	PLPI118	?	0	0	0	1
119	*Pinnularia divergens var subcapitata* Frenguelli	PLPI119	1	0	0	0	1
120	*Pinnularia graciliodes var. rumrichae* Krammer	PLPI120	0	0	0	0	1
121	*Pinnularia nov* sp. 18	PLPI121	1	0	0	0	1
122	*Pinnularia nov sp.* 2	PLPI122	1	0	0	0	1
123	*Pinnularia nov sp.* 5.1	PLPI123	1	0	0	0	1
124	*Pinnularia patagonensis* Lange-Bertalot & Metzeltin	PLPI124	1	0	0	0	1
125	*Pinnularia spathulata* (Frenguelli)	PLPI125	1	0	0	0	1
126	*Pinnularia subinterrupta* Krammer & Schroeter	PLPI126	0	0	0	0	1
127	*Pinnularia viridiformis* Krammer	PLPI127	0	0	0	0	1
128	*Placoneis elginensis* (Greg.) Cox	PLPL128	0	0	0	0	1
129	*Placoneis exiguiformis* (Hustedt) Lange-Bertalot	PLPL129	0	0	0	0	1
130	*Placoneis symmetrica* (Hustedt) Lange-Bertalot	PLPL130	0	0	0	0	1
131	*Planothidium aueri* (Krasske) Lange-Bertalot	PSPL131	1	0	0	0	1
132	*Planothidium lanceolatum* (Brébisson ex Kützing) Lange-Bertalot	PSPL132	0	0	0	0	1
133	*Planothidium sp1*	PSPL133	?	0	0	0	1
134	*Pseudostaurosira aff. microstriata* (Marciniak) Flower	FSPS134	?	0	0	1	0
135	*Pseudostaurosira australopatagonica* García, Villacís, Maidana & Morales	FSPS135	1	0	0	1	0
136	*Pseudostaurosira tenuis* Morales et M.B. Edlund	FSPS136	0	0	0	1	0
137	*Pseudostaurosiropsis aff. geocollegarum* (Witkowski & Lange-Bertalot) Morales	FSPS137	?	0	0	1	0
138	*Rhoicosphenia abreviata* (Agardh) Lange-Bertalot	PLRH138	0	0	0	0	1
139	*Rhopalodia acuminata* Krammer	HLRH139	0	0	0	0	1
140	*Rhopalodia gibba var gibba* (Ehrenberg) O. Müller	HLRH140	0	0	0	0	1
141	*Sellaphora* [*laevissima* K-LB] aff. Φ 'normal' sensu Mann 2008	PLSE141	0	0	0	0	1
142	*Sellaphora* [*pupula* K-LB] aff. Φ 'cf. large' sensu Mann 2008	PLSE142	0	0	0	0	1
143	*Sellaphora* [*pupula* K-LB] aff. Φ 'pseudocapitate' sensu Mann 2008	PLSE143	0	0	0	0	1
144	*Sellaphora nigri* (De Not) Weztel et Ector sensu Wetzel	PSSE144	0	0	0	0	1
145	*Sellaphora seminulum* Grunow	PSSE145	0	0	0	0	1
146	*Stauroforma exiguiformis* (Lange-Bertalot) R.J. Flower, V.J. Jones & Round	FSST146	0	0	0	1	0
147	*Stauroneis bryocola* Van de Vijver & Lange-Bertalot	PLST147	1	0	0	0	1
148	*Stauroneis fuegiana* Casa & Van de Vijver	PLST148	1	0	0	0	1
149	*Stauroneis gracilior* Reichardt 1995	PLST149	0	0	0	0	1

150	*Stauroneis heinii* Lange-Bertalot & Krammer 1999	PLST150	0	0	0	0	1
151	*Staurosira aff. longwanensis* Rioual, E. Morales et Ector	FSST151	?	0	0	1	0
152	*Staurosira aff. venter* (Ehrenberg) Cleve & Möller	FSST152	?	0	0	1	0
153	*Staurosira dimorpha* E.A. Morales, M.B. Edlund & S.A. Spaulding	FSST153	?	0	0	1	0
154	*Staurosirella aff. dubia* (Grunow) Morales & Manoylov	FSST154	?	0	0	1	0
155	*Surirella biseriata* Brébisson	PLSU155	0	1	0	0	1
156	*Tabellaria ventricosa* Kützing	PLTA156	0	0	0	0	0
157	*Urosolenia sp1*	CSUR157	?	1	0	0	0
158	*Veigaludwigia urbana* (Krasske) Lange-Bertlot	PLVE158	1	0	0	0	1
159	*Staurosirella leptostauron* (Ehrenberg) D.M.Williams & Round 1988	FSST159	0	0	0	1	0
160	*Stauroforma sp1*	FSXX160	?	0	0	1	0

Discussion on the autoecology of *Aulcoseira humilis/liucoensis*

A commonality between *Aulcoseira humilis* and *Aulacoseira liucoensis* is their temperate to subpolar distribution, where *A. liucoensis*, although recently published (García et al., 2019), has a reported distribution limited to Patagonia, spanning from 39°S to 50°S, and *A. humilis* a distribution limited to the northern regions of Eurasia and north America (48°N – 70°N). The presence of both taxa in LC thus expands their austral-most extension. Both, although rarely sighted, are associated with similar limnologic and climatic parameters, which are reported to be the following: *A. humilis* residing in oligotrophic, shallow lakes (except for Lake Frolikha and Lake Imandra), with pH between 5 and 9.2, although more frequently circumneutral, and precipitation ranging from 200 to 1070 mm/yr, temperature ranging from -36°C to 16.1°C, and altitude between 7 to 524 masl (Stevenson et al., 1991; Siver and King, 1997; Trifonova and Genkal, 2000; Enache and Prarie, 2000; Laing and Smol, 2003; Genkal and Kulikovskiy, 2014; Denisov and Genkal 2018; Neil et al., 2019), and *A. liucoensis* occupying oligotrophic, relatively shallow lakes, with circumneutral pH ranging between 6.8 and 7.7, and precipitation ranging from 300 to 930 mm/yr, temperature from -9.3 to 17.4 °C, and altitude between 539 and 1090

masl (Fey et al., 2009; Mayr et al., 2019; García et al., 2019). Unstratified conditions and/or wind-driven turbulence accompanied by ice-free lake-surface has also been associated with these taxa as necessary prerequisites for their proliferation. Although overlap exists between these taxa, in vague terms, *A. liucoensis* is most common in the older portion of the record and *A. humilis* in the younger (<~4 ka). Their similar autoecological preferences - known so far- makes their grouping suitable.

To further disentangle the ecological meaning of *Aulacoseira humilis/liucoensis*, relevant case studies are those of Middendorf lake (Laing and Smol, 2003) and Lake Stowell (Neil et al., 2019), as they present similar multimillennial-scale interplay between small fragilarioid and *Aulacoseira* dominance (specifically including *A. humilis*) in these records. These are small, isolated lakes spread across a broad latitudinal transect affected by glaciation, in which their ontogeny has been discussed in terms of fluctuating levels of these taxa. The reasons proposed for surges of *Aulacoseira* are varied but linger around wind-driven turbulence, thermal instability, and/or enhanced catchment input. On one hand, the limnological conditions of Middendorf lake (70°22'N, 87°33' E; ~90 masl; 200-400 mm/yr; -32 to 8°C [mean winter and summer]) are most susceptible to changes in the duration of the freezing season, as this restricts or permits the occupation of the water column by plankton and *Aulacoseira*. On the other hand, Lake Stowell (48°46' N, 123°26' W; 70 masl; 1070 mm/yr; 2.8 to 16.1°C [mean winter and summer]) is most susceptible to changes related to higher thermal stratification which favors obligate plankton over heavily silicified tychoplankton (i.e., *Aulacoseira*). In the former, *Aulacoseira* as opposed to small fragilarioid dominance was linked to ameliorating climate conditions, prolonging ice-free water column mixing, while in the later, this taxon, as opposed to planktonic or small fragilarioid proliferation, was linked to warming early-Holocene temperatures under total phosphorous

limited lake conditions accompanied by open-canopy surroundings that may have facilitated wind-driven mixing, and afterwards to cooling mid-Holocene temperatures that may have weakened the lake thermal stratification synchronous to the biogeochemical coupling of terrestrial succession and limnological conditions. The ambivalent nature of *Aulacoseira* revealed in the second case (Lake Stowell) is resolved by different *Aulacoseira spp.* being represented during the early and mid-Holocene intervals, when *Aulacoseira humilis* is most prominent during the mid- to late-Holocene interval. LC presents conditions somewhere in between these two examples (~700 mm/yr; 3.1 to 11.7 °C [mean winter and summer]), corroborating that *Aulacoseira* dominant intervals indicate turbulence of some sort - via physical or thermal mixing – as well as considerably long ice-free seasons with sparse macrophyte cover (Vermaire and Gregory-Eaves, 2007). These are to be considered as the mean limnological conditions in LC.

Age-Depth model of PS0710

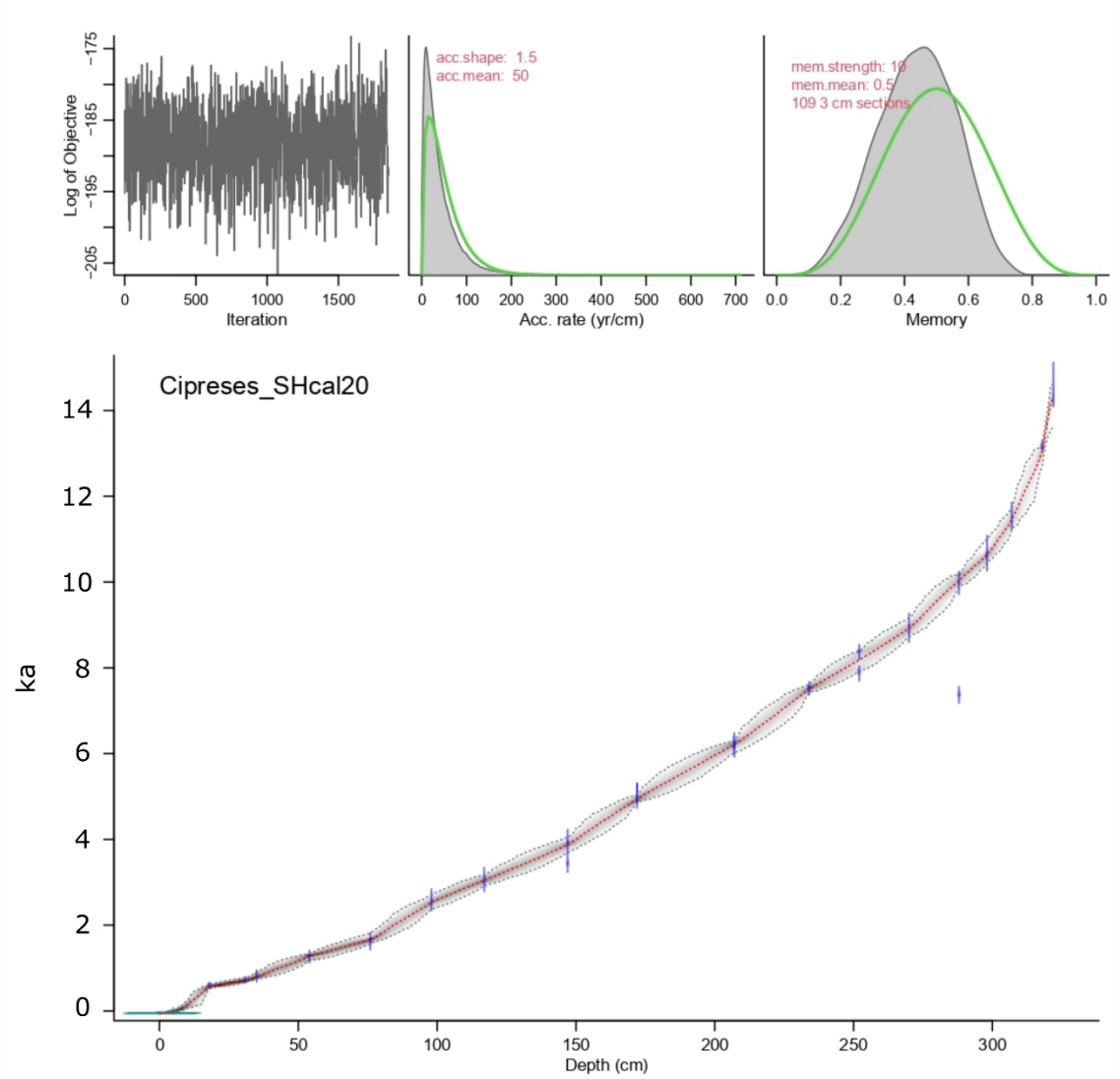

Figure S1. Age-depth model of sedimentary core PS0710, calibrated with SHcal20. Model was generated with R Bacon package. Radiocarbon dates may be found in Moreno et al., 2018c.